CrossMark

J. Fluid Mech. (2016), *vol.* 793, *pp.* 877–914. © Cambridge University Press 2016
doi:10.1017/jfm.2016.155

Solute dispersion in pulsatile Casson fluid flow in a tube with wall absorption

Jyotirmoy Rana[1,†] **and P. V. S. N. Murthy**[1]

[1]Department of Mathematics, Indian Institute of Technology, Kharagpur 721302, India

(Received 31 March 2015; revised 19 January 2016; accepted 20 February 2016;
first published online 23 March 2016)

The analysis of axial dispersion of solute is presented in a pulsatile flow of Casson fluid through a tube in the presence of interfacial mass transport due to irreversible first-order reaction catalysed by the tube wall. The theory of dispersion is studied by employing the generalized dispersion model proposed by Sankarasubramanian & Gill (*Proc. R. Soc. Lond.* A, vol. 333 (1592), 1973, pp. 115–132). This dispersion model describes the whole dispersion process in terms of three effective transport coefficients, i.e. exchange, convection and dispersion coefficients. In the present study, the effects of yield stress of Casson fluid τ_y, wall absorption parameter β, amplitude of fluctuating pressure component e and Womersley frequency parameter α on the dispersion process are discussed under the influence of pulsatile pressure gradient. In a pulsatile flow, the plug flow radius changes during the period of oscillation and it has an effect on the dispersion process. Even with the Casson fluid model also, in an oscillatory flow, for small values of α, the dispersion coefficient K_2 is positive, but when the value of α is as large as 3, K_2 takes both positive and negative values due to the fluctuations in the velocity profiles. This nature becomes more predominant for τ_y, e and β. It is observed that initially, for small time, the amplitude and magnitude of fluctuations of K_2 becomes more rapid and increases with time but it decreases after certain time and reaches a non-transient state for large time. Like in the case of Newtonian model, double frequency period for K_2 is observed at small time for large values of α with the Casson model for blood. It is seen that critical time for which K_2 reaches a non-transient state is independent of τ_y and e but is dependent on α. It is also observed that the axial distribution of mean concentration C_m of solute depends on τ_y and β. But the effect of e and α on C_m is not very significant. This dispersion model in non-Newtonian pulsatile flow can be applied to study the dispersion process in the cardiovascular system and blood oxygenators.

Key words: blood flow, rheology

1. Introduction

The study of axial dispersion of a solute with the effect of boundary absorption in a straight tube has always been an interesting topic of research due to its broad applications in the fields of environmental dynamics, chemical engineering, biomedical engineering and physiological fluid dynamics. Related to the theory of dispersion,

† Email address for correspondence: jyotirmoy.rana@gmail.com

https://doi.org/10.1017/jfm.2016.155 Published online by Cambridge University Press

some examples are the pollutant transport in the environment, chromatographic separations in chemical engineering, the mixing and the transportation of drugs or toxins in physiological systems.

At first, Taylor (1953) introduced the method of solute dispersion in a steady laminar viscous fluid flow through a straight tube, analytically and experimentally. In this study, it was discussed that solute in the fluid is dispersed due to both radial molecular diffusion and the axial convection with the effective molecular diffusion coefficient, D_{eff}, defined by $D_{eff} = R^2 w_m^2/48D_m$, where D_m is molecular diffusivity, w_m is the mean axial velocity and R is the radius of the tube. A new approach to study on Taylor dispersion in steady flow was described by Aris (1956) using the method of moments. In this analysis, the asymptotic behaviour of second moment about the mean was analysed by incorporating the effect of axial molecular diffusion with the effective molecular diffusion coefficient, D_{eff}, defined by $D_{eff} = D_m + R^2 w_m^2/48D_m$. The axial dispersion of solute in a pulsatile flow of viscous fluid through an infinitely long tube with the pulsating pressure gradient was investigated by Aris (1960) using the method of moments. These studies were analysed only on the dispersion of solute at large times after the injection in the fluid but did not give any information about the solute dispersion for small times after the injection. After that Gill & Sankarasubramanian (1970) proposed a generalized dispersion model for fully developed steady laminar flow in a tube which provides the idea of solute dispersion at each time after injection of solute in the fluid. Using this method of analysis, the study of solute dispersion with the effect of interphase mass transfer across the tube wall was analysed by Sankarasubramanian & Gill (1973) under the consideration of three effective transport coefficients i.e. exchange coefficient due to the irreversible first-order reaction at the tube wall, convective coefficient due to velocity of the solute and dispersion coefficient due to the molecular diffusion and the velocity of the fluid. This dispersion model is much more applicable in wide area of unsteady state heat and mass transfer problems.

Several researchers have applied the Taylor–Aris's dispersion theory and the generalized dispersion model to analyse the dispersion process of solute in steady and oscillatory flows in the Newtonian fluid through a straight and curved tube or channel or annulus with and without the effect of absorption or irreversible first-order catalytic reaction at the boundary. The longitudinal dispersion of passive contaminant in oscillatory flows through a tube with an effective molecular diffusion coefficient, D_{eff} was discussed by Chatwin (1975). Experimental results for axial transport of contaminant gas in oscillatory flow in a tube were obtained by Joshi *et al.* (1983) to determine the effective molecular diffusion coefficient. Rao & Deshikachar (1987) studied the axial dispersion of solute in a fully developed laminar steady flow through an annular pipe. The axial dispersion of a passive contaminant in a pulsatile flow of viscous incompressible fluid with the effect of first-order irreversible catalytic reaction at the tube wall was analysed by Mazumder & Das (1992) following the method of moments. Using the Aris–Barton method of moments, Bandyopadhyay & Mazumder (1999) developed a dispersion model to study the effect of longitudinal dispersion process for the pulsatile flow in a channel. Based on the generalized dispersion model, the study of solute dispersion in a periodic flow through an annulus with the effect of irreversible boundary reaction was described by Sarkar & Jayaraman (2004). By introducing the method of integral moments, Mazumder & Mondal (2005) discussed

https://doi.org/10.1017/jfm.2016.155 Published online by Cambridge University Press

on the dispersion process of passive tracer under the combined effects of frequency of pressure pulsation and first-order heterogeneous chemical reaction at the outer wall in a pulsatile flow through an annular pipe. The combined effects of heterogeneous reversible and irreversible wall reactions on dispersion of a chemical species in steady and oscillatory flows in a small diameter tube were studied by Ng (2006) using the multiple scale asymptotic analysis. The unsteady longitudinal dispersion of solute in oscillatory flow through a curved channel with absorbing walls using the Aris–Barton method of moments was analysed by Kumar & Jayaraman (2008). Imposing the method of integral moments, the analysis of longitudinal dispersion of solute in a periodic flow between two coaxial cylinders was presented by Paul (2011) to determine the longitudinal dispersion coefficient with the various of radius ratio, absorption parameter and frequency parameter.

The study of solute dispersion in an unsteady flow of non-Newtonian fluids has lots of applications in polymers, biochemical processing and cardiovascular flows. But little literature on dispersion processes can be found on non-Newtonian fluids. Following the theory of Taylor's dispersion, the effective axial diffusion coefficient was determined by Sharp (1993) in fully developed steady flow of non-Newtonian fluids such as Casson, power law and Bingham fluids in a straight tube. Based on Taylor's dispersion model, the axial dispersion of solute in power law fluids through a circular curved tube was analysed by Agrawal & Jayaraman (1994) for low Dean number, Dn, defined by $Dn = Re/\sqrt{\lambda}$, where Re is the Reynolds number based on diameter of the tube and λ is the curvature ratio. Hazra, Gupta & Niyogi (1997) presented a literature on solute dispersion in oscillatory flow of a viscoelastic non-Newtonian second-order fluid through a channel to obtain the longitudinal dispersion coefficient with the effects of viscoelastic parameter, amplitude and frequency of pressure pulsation by using the generalized dispersion model. Dash, Jayaraman & Mehta (2000) extended the study of Sharp (1993) for unsteady solute dispersion in a Casson fluid in a pipe and channel under the presence of effective diffusion coefficient and the effect of yield stress of the fluid by using the approach of generalized dispersion model. The solute dispersion in a Casson fluid flow in a pipe and channel with the combined effect of yield stress and irreversible wall reaction was analysed by Nagarani, Sarojamma & Jayaraman (2004) using the generalized dispersion model. This study was extended by Nagarani, Sarojamma & Jayaraman (2009) in a Casson fluid flow in an annulus which has an application to catheterized artery under the presence of boundary reaction. But these studies of Nagarani *et al.* (2004, 2009) were found to be applicable only for large time after the injection of the solute. Nagarani, Sarojamma & Jayaraman (2006) described the dispersion process of solute in the flow of a Casson fluid in an annulus by employing the generalized dispersion model with the effects of the yield stress and the annular gap. Applying the generalized dispersion model, the analysis of unsteady solute dispersion in the pulsatile flow of a Casson fluid in a tube was presented by Nagarani & Sebastian (2013) to determine the dispersion coefficient and the concentration of solute with the effects of Womersley frequency number, Schmidt number, yield stress and fluctuating pressure component. In this study, the effect of first-order reaction catalysed by the tube wall on the dispersion process has not been discussed.

In the present study, the unsteady axial dispersion of solute in the pulsatile flow of a non-Newtonian Casson fluid in a tube is analysed with the effect of an irreversible first-order boundary reaction. By following the generalized dispersion model proposed by Gill & Sankarasubramanian (1970) and Sankarasubramanian & Gill (1973), the solute transport in the fluid is analysed by considering three effective transport

https://doi.org/10.1017/jfm.2016.155 Published online by Cambridge University Press

coefficients i.e. exchange, convection and dispersion coefficients. From this analysis, it is noticed that the convection and dispersion coefficient not only depend on time but also depend on the wall absorption parameter, yield stress, amplitude of fluctuating pressure component and Womersley frequency parameter in the presence of boundary reaction. The axial mean concentration of solute is also discussed with the effect of the boundary reaction, time, yield stress, fluctuating pressure component and frequency parameter. This study on dispersion process has wide application of blood flows due to pulsatile nature of the flow of blood (Nagarani *et al.* 2004).

2. Mathematical formulation

An unsteady, axisymmetric, fully developed, pulsatile flow of Casson fluid in a straight circular cylindrical tube of radius R as shown in figure 1 is considered to analyse the axial dispersion of solute. In this study, one-dimensional flow is assumed. Due to an irreversible first-order catalytic reaction, solute is continuously absorbed by the tube wall and the rate of solute absorption is proportional to the solute concentration at the wall. In this study, free convection effects are neglected and a dilute solution is considered so that the product of reaction does not cause any coupling of flux (Sankarasubramanian & Gill 1973).

2.1. *Governing equation*

The concentration of the solute is analysed by the unsteady convective diffusion equation

$$\frac{\partial C'}{\partial t'} + w'(t', r')\frac{\partial C'}{\partial z'} = D_m\left(\frac{1}{r'}\frac{\partial}{\partial r'}\left(r'\frac{\partial C'}{\partial r'}\right) + \frac{\partial^2 C'}{\partial z'^2}\right), \tag{2.1}$$

where C' is the local concentration of the solute, w' is the axial velocity of the fluid in tube, D_m is the molecular diffusivity, t' is the time and r' and z' represent the radial and axial directions, respectively.

2.2. *Initial and boundary conditions*

(I) Initial condition:

Following Sankarasubramanian & Gill (1973), the initial solute distribution at $t' = 0$ is considered by introducing the solute of mass M at the plane $z' = 0$ in a circular tube over the circular cross-section of radius R. Hence, the initial concentration distribution may be written as

$$C'(0, z', r') = C_0\psi_1(z')Y_1(r'), \tag{2.2}$$

with

$$C_0 = \frac{M}{\pi R^3}, \tag{2.3}$$

$$\psi_1(z') = R\delta(z'), \tag{2.4}$$

and

$$Y_1(r') = 1, \tag{2.5}$$

where $\delta(z')$ is the Dirac delta function.

https://doi.org/10.1017/jfm.2016.155 Published online by Cambridge University Press

(II) Boundary conditions:

The following three boundary conditions are relevant for the present study.

(i) Condition due to symmetry

$$\frac{\partial C'}{\partial r'}(t', z', 0) = 0. \tag{2.6}$$

(ii) Condition due to the irreversible first-order heterogeneous reaction at the tube wall

$$-D_m \frac{\partial C'}{\partial r'}(t', z', R) = kC'(t', z', R), \tag{2.7}$$

where k is the reaction rate constant.

(iii) Since the amount of solute in the system is finite, we shall have

$$C'(t', \infty, r') = \frac{\partial C'}{\partial z'}(t', \infty, r') = 0. \tag{2.8}$$

2.3. *Constitutive equation for Casson fluid and momentum equation*

Following Aroesty & Gross (1972), the constitutive equation for Casson fluid in one dimensional shear flow may be written as

$$\tau'^{1/2} = \tau_y'^{1/2} + \left(-\mu \frac{\partial w'}{\partial r'}\right)^{1/2}, \quad \text{if } \tau' \geqslant \tau_y', \tag{2.9a}$$

$$\frac{\partial w'}{\partial r'} = 0, \quad \text{if } \tau' \leqslant \tau_y', \tag{2.9b}$$

where τ' and $\partial w'/\partial r'$ are the shear stress and shear rate, respectively, τ_y' is the yield stress, and μ is the viscosity of Casson fluid (viscosity at high shear rate).

In the plug flow region in which shear stress τ' is less than yield stress τ_y', the velocity gradients become zero. When shear rates in the fluid become very high i.e. for $\tau' > \tau_y'$, Newtonian behaviour induces in the fluid. This behaviour is related to the blood flow in small tubes (Aroesty & Gross 1972). The yield stress of the human blood is typically 0.04 dyn cm^{-2} at a hematocrit of 40 % (Merrill 1969).

Due to the pulsatile flow, the pressure gradient at any z' is represented by

$$-\frac{\partial p'}{\partial z'}(t') = P_0 + P_1 \sin(\omega t'), \tag{2.10}$$

where P_0 and P_1 are the steady and fluctuating components of the pressure gradient acting along the axis of tube, ω is the frequency of the pressure pulsation.

The momentum equation for Casson fluid is represented as

$$\rho \frac{\partial w'}{\partial t'} = -\frac{\partial p'}{\partial z'} - \frac{1}{r'} \frac{\partial}{\partial r'}(r'\tau'), \tag{2.11}$$

with boundary conditions

$$\tau' \text{ is finite} \quad \text{at } r' = 0 \tag{2.12}$$

and

$$w' = 0 \quad \text{at } r' = R. \tag{2.13}$$

https://doi.org/10.1017/jfm.2016.155 Published online by Cambridge University Press

2.4. *Non-dimesionalization and velocity distribution*

By introducing the following non-dimensional variables

$$\left.\begin{gathered} C=\frac{C'}{C_0},\quad w=\frac{w'}{w_0},\quad r=\frac{r'}{R},\quad z=\frac{D_m z'}{R^2 w_0},\\ t=\frac{D_m t'}{R^2},\quad \tau=\frac{\tau'}{\mu(w_0/R)},\quad \tau_y=\frac{\tau_y'}{\mu(w_0/R)},\quad e=\frac{P_1}{P_0}, \end{gathered}\right\} \tag{2.14}$$

the governing equation (2.1) transforms to

$$\frac{\partial C}{\partial t}+w(t,r)\frac{\partial C}{\partial z}=\frac{1}{r}\frac{\partial}{\partial r}\left(r\frac{\partial C}{\partial r}\right)+\frac{1}{Pe^2}\frac{\partial^2 C}{\partial z^2}, \tag{2.15}$$

where $w_0=(R^2/4\mu)P_0$ is the characteristic velocity, and $Pe=Rw_0/D_m$ is the Peclet number.

The initial condition (2.2) and boundary conditions (2.6)–(2.8) can be written in non-dimensional form as:

$$C(0,z,r)=\psi(z)Y(r), \tag{2.16}$$

with

$$\psi(z)=\delta(z)/Pe, \tag{2.17}$$

and

$$Y(r)=1, \tag{2.18}$$

$$\frac{\partial C}{\partial r}(t,z,0)=0, \tag{2.19}$$

$$\frac{\partial C}{\partial r}(t,z,1)=-\beta C(t,z,1), \tag{2.20}$$

$$C(t,\infty,r)=\frac{\partial C}{\partial z}(t,\infty,r)=0, \tag{2.21}$$

where $\beta=kR/D_m$ is the wall absorption parameter.

Using the non-dimensional variables, the constitutive equation (2.9) reduces to

$$\tau^{1/2}=\tau_y^{1/2}+\left(-\frac{\partial w}{\partial r}\right)^{1/2},\quad \text{if } \tau\geqslant\tau_y, \tag{2.22a}$$

$$\frac{\partial w}{\partial r}=0,\quad \text{if } \tau\leqslant\tau_y. \tag{2.22b}$$

The momentum equation (2.11) in non-dimensional form is given by

$$\varepsilon\frac{\partial w}{\partial t}=2p(t)-\frac{1}{r}\frac{\partial}{\partial r}(r\tau), \tag{2.23}$$

with boundary conditions

$$\tau \text{ is finite} \quad \text{at } r=0 \tag{2.24}$$

and

$$w=0 \quad \text{at } r=1, \tag{2.25}$$

where $\varepsilon=1/Sc$, $p(t)=-2(\partial p'/\partial z')/P_0$, $Sc=\nu/D_m$ is the Schmidt number and ν is the kinematic viscosity coefficient.

https://doi.org/10.1017/jfm.2016.155 Published online by Cambridge University Press

Since the Schmidt number is very large ($O(10^3)$) in arterial blood flows (Caro *et al.* 1978), the parameter ε is very small. In this study, ε is treated as a perturbation parameter to obtain the velocity distribution for small as well as large values of Womersley frequency parameter α. Because of large values of Sc, it is more appropriate to use this non-dimensionalization instead of the one that was given in Nagarani & Sebastian (2013).

By solving the nonlinear coupled equations (2.22) and (2.23) with perturbation analysis for small parameter ε, the velocity distribution (Aroesty & Gross 1972) in the plug flow region ($0 \leqslant r \leqslant r_p$) is obtained as

$$w_1 = \frac{p(t)}{2}\left[1 - \frac{8}{3}r_p^{1/2} + 2r_p - \frac{1}{3}r_p^2\right] - \varepsilon\frac{p'(t)}{32}\left[3 - \frac{1144}{147}r_p^{1/2} + \frac{320}{63}r_p + \frac{4}{3}r_p^2 - \frac{16}{9}r_p^{5/2} + \frac{65}{441}r_p^4\right], \quad \text{if } 0 \leqslant r \leqslant r_p, \tag{2.26a}$$

and that in the outside of plug region ($r_p \leqslant r \leqslant 1$) is obtained as

$$\begin{aligned} w_2 = {} & \frac{p(t)}{2}\left[(1-r^2) - \frac{8}{3}r_p^{1/2}(1-r^{3/2}) + 2r_p(1-r)\right] \\ & - \varepsilon\frac{p'(t)}{2}\left[\frac{3}{16} - \frac{r^2}{16}(4-r^2) - \frac{r_p^{1/2}}{16}\left(\frac{1144}{147} - \frac{16}{3}(r^2 + r^{3/2}) + \frac{424}{147}r^{7/2}\right)\right] \\ & - \varepsilon p'(t)\frac{r_p}{32}\left[\frac{320}{63} + \frac{128}{63}r^3 - \frac{64}{9}r^{3/2}\right], \quad \text{if } r_p \leqslant r \leqslant 1. \end{aligned} \tag{2.26b}$$

In the above equations for velocity, $p(t) = 2(1 + e\sin(\alpha^2 Sc\, t))$, $\alpha^2 = \omega R^2/(\mu/\rho)$, α is known as Womersley frequency parameter, e is the amplitude of the fluctuating pressure component, $r_p = \tau_y/p(t)$ is the dimensionless radius of the plug flow region and $p'(t) = \mathrm{d}p/\mathrm{d}t$. The product $\alpha^2 Sc$ is the ratio of characteristic time of diffusion to the period of oscillation.

3. Method of solution

The unsteady convective diffusion equation (2.15) along with the initial and boundary conditions (2.16)–(2.21) is solved using the method suggested in Sankarasubramanian & Gill (1973). The solute concentration $C(t, z, r)$ is expanded in an infinite series as

$$C(t, z, r) = \sum_{i=0}^{\infty} f_i(t, r)\frac{\partial^i C_m(t, z)}{\partial z^i}, \tag{3.1}$$

where the dimensionless mean concentration $C_m(t, z)$ is defined by

$$C_m(t, z) = 2\int_0^1 Cr\,\mathrm{d}r, \tag{3.2}$$

and f_i $(i = 0, 1, 2, \ldots)$ are functions of t and r.

https://doi.org/10.1017/jfm.2016.155 Published online by Cambridge University Press

After multiplying by $2r$ and integrating with respect to r from 0 to 1, the non-dimensional form of the governing equation (2.15) can be rewritten as

$$\frac{\partial C_m}{\partial t} = \frac{1}{Pe^2}\frac{\partial^2 C_m}{\partial z^2} + 2\frac{\partial C}{\partial r}(t, z, 1) - 2\frac{\partial}{\partial z}\int_0^1 w(t, r)C(t, z, r)r\,\mathrm{d}r. \tag{3.3}$$

By substituting (3.1) into (3.3), the following dispersion model for C_m is derived:

$$\frac{\partial C_m}{\partial t} = \sum_{i=0}^{\infty} K_i(t)\frac{\partial^i C_m}{\partial z^i}, \tag{3.4}$$

where

$$K_i(t) = \frac{\delta_{i2}}{Pe^2} + 2\frac{\partial f_i}{\partial r}(t, 1) - 2\int_0^1 f_{i-1}(t, r)w(t, r)r\,\mathrm{d}r, \quad i = 0, 1, 2, \ldots, \tag{3.5}$$

and δ_{ij} denotes Kronecker delta

$$\delta_{ij} = \begin{cases} 1, & i = j, \\ 0, & i \neq j. \end{cases} \tag{3.6}$$

In (3.4), the terms involving $K_i(t)$ $(i = 3, 4, 5, \ldots)$ can be neglected as their contribution is not significant (Gill & Sankarasubramanian 1970). Then the resulting generalized dispersion model for mean concentration $C_m(t, z)$ is represented as

$$\frac{\partial C_m}{\partial t} = K_0(t)C_m + K_1(t)\frac{\partial C_m}{\partial z} + K_2(t)\frac{\partial^2 C_m}{\partial z^2}, \tag{3.7}$$

where

$$K_i(t) = \frac{\delta_{i2}}{Pe^2} + 2\frac{\partial f_i}{\partial r}(t, 1) - 2\int_0^1 f_{i-1}(t, r)w(t, r)r\,\mathrm{d}r, \quad i = 0, 1, 2. \tag{3.8}$$

In this study, $K_0(t)$, $K_1(t)$, and $K_2(t)$ are the exchange coefficient due to non-zero solute flux at the tube wall, convection coefficient due to the velocity of solute and dispersion coefficient due to the molecular diffusion and the velocity of the fluid, respectively. Due to the presence of pulsatile flow, both the coefficients $K_1(t)$ and $K_2(t)$ are the periodic functions of time (Chatwin 1975; Sarkar & Jayaraman 2004).

Now the solute concentration $C(t, z, r)$ can be expanded in a finite series as

$$C(t, z, r) = \sum_{i=0}^{2} f_i(t, r)\frac{\partial^i C_m(t, z)}{\partial z^i}. \tag{3.9}$$

Substituting (3.7) and (3.9) into (2.15), and equating the coefficients of $\partial^n C_m/\partial z^n$ $(n = 0, 1, 2)$, the set of differential equations for f_n are obtained as

$$\frac{\partial f_n}{\partial t} = \frac{1}{r}\frac{\partial}{\partial r}\left(r\frac{\partial f_n}{\partial r}\right) - w(t, r)f_{n-1} + \frac{1}{Pe^2}f_{n-2} - \sum_{i=0}^{n} K_i(t)f_{n-i}, \tag{3.10}$$

where $n = 0,\ 1,\ 2,$ and $f_{-1} = f_{-2} = 0$.

https://doi.org/10.1017/jfm.2016.155 Published online by Cambridge University Press

Using (3.2) and (3.9) in the initial and boundary conditions (2.16)–(2.21), the coefficients C_m and f_n are expressed as

$$C_m(0, z) = 2\psi(z) \int_0^1 Y(r) r \, \mathrm{d}r, \tag{3.11}$$

$$f_0(0, r) = \frac{Y(r)}{2 \displaystyle\int_0^1 Y(r) r \, \mathrm{d}r}, \tag{3.12}$$

$$f_n(0, r) = 0, \quad n = 1, 2, \tag{3.13}$$

$$\frac{\partial f_n}{\partial r}(t, 0) = 0, \quad n = 0, 1, 2, \tag{3.14}$$

$$\frac{\partial f_n}{\partial r}(t, 1) = -\beta f_n(t, 1), \quad n = 0, 1, 2, \tag{3.15}$$

and

$$C_m(t, \infty) = \frac{\partial C_m}{\partial z}(t, \infty) = 0. \tag{3.16}$$

Now using the definition of mean concentration $C_m(t, z)$ defined by (3.2) into (3.9), we have

$$\int_0^1 f_n(t, r) r \, \mathrm{d}r = \frac{1}{2}\delta_{n0}, \quad n = 0, 1, 2, \tag{3.17}$$

where δ_{n0} denotes as Kronecker delta described in (3.6).

The unknown functions f_0, K_0, f_1, K_1, f_2 and K_2 are obtained by solving the coupled system of partial differential equations (3.8) and (3.10). The method of eigenfunction expansion is used to determine the effective transport coefficients K_i, $i = 0, 1, 2$.

3.1. *Estimation of $f_0(t, r)$ and $K_0(t)$*

The equation involving $f_0(t, r)$ and exchange coefficient $K_0(t)$ can be written from (3.10) as

$$\frac{\partial f_0}{\partial t} = \frac{1}{r}\frac{\partial}{\partial r}\left(r \frac{\partial f_0}{\partial r}\right) - f_0 K_0, \tag{3.18}$$

with the initial and boundary conditions (3.12), (3.14), (3.15) for $n = 0$, and an additional condition obtained from (3.17) as

$$\int_0^1 f_0(t, r) r \, \mathrm{d}r = \frac{1}{2}. \tag{3.19}$$

Using the method of eigenfunction expansion, the solution of non-homogeneous boundary value problem (3.18) for $f_0(t, r)$ satisfying the initial and boundary conditions (3.12), (3.14), (3.15) and the condition (3.19) is obtained as (Boyce, DiPrima & Haines 1992)

$$f_0(t, r) = \frac{\displaystyle\sum_{n=0}^{\infty} A_n \mathrm{J}_0(\mu_n r) \mathrm{e}^{-\mu_n^2 t}}{2 \displaystyle\sum_{n=0}^{\infty} (A_n/\mu_n) \mathrm{J}_1(\mu_n) \mathrm{e}^{-\mu_n^2 t}}, \tag{3.20}$$

https://doi.org/10.1017/jfm.2016.155 Published online by Cambridge University Press

where J_0 and J_1 are the Bessel functions of the first kind of order zero and one, respectively and μ_n are the roots of transcendental equation

$$\mu_n J_1(\mu_n) = \beta J_0(\mu_n), \quad n = 0, 1, 2, \ldots \tag{3.21}$$

and

$$A_n = \frac{\mu_n^2 \int_0^1 rY(r) J_0(\mu_n r)\, dr}{(\mu_n^2 + \beta^2) J_0^2(\mu_n) \int_0^1 rY(r)\, dr}, \quad n = 0, 1, 2, \ldots. \tag{3.22}$$

From (3.8) and (3.20)–(3.22), we obtain the exchange coefficient $K_0(t)$ as

$$K_0(t) = 2\frac{\partial f_0}{\partial r}(t, 1) = -\frac{\sum_{n=0}^{\infty} A_n \mu_n J_1(\mu_n) e^{-\mu_n^2 t}}{\sum_{n=0}^{\infty} (A_n/\mu_n) J_1(\mu_n) e^{-\mu_n^2 t}}, \tag{3.23}$$

which is exactly the same as derived by Sankarasubramanian & Gill (1973). It is seen that $K_0(t)$ is independent of velocity field.

3.2. *Estimation of $f_1(t, r)$ and $K_1(t)$*

The governing equation for $f_1(t, r)$ and the convection coefficient $K_1(t)$ is derived from (3.10) by taking $n = 1$ and is written as

$$\frac{\partial f_1}{\partial t} = \frac{1}{r}\frac{\partial}{\partial r}\left(r\frac{\partial f_1}{\partial r}\right) - f_1 K_0 - (w(t, r) + K_1) f_0. \tag{3.24}$$

The appropriate initial and boundary conditions are given in (3.13)–(3.15) and we have also an additional condition obtained from (3.17) as

$$\int_0^1 f_1(t, r) r\, dr = 0. \tag{3.25}$$

The eigenfunction expansion solution for $f_1(t, r)$ satisfying the initial and boundary conditions (3.13)–(3.15) and the condition (3.25) is obtained as

$$f_1(t, r) = -\frac{\sum_{n=0}^{\infty} \left[\sum_{m=0}^{\infty} B_{1mn} \left(\int_0^t e^{-(\mu_m^2 - \mu_n^2)s} D_{mn}(s)\, ds\right) + B_{2n} F_1(t)\right] J_0(\mu_n r) e^{-\mu_n^2 t}}{2\sum_{n=0}^{\infty} (A_n/\mu_n) J_1(\mu_n) e^{-\mu_n^2 t}}, \tag{3.26}$$

https://doi.org/10.1017/jfm.2016.155 Published online by Cambridge University Press

where

$$F_1(t) = \int_0^t K_1(s)\,\mathrm{d}s$$
$$= -\frac{\displaystyle\sum_{n=0}^{\infty}\sum_{m=0}^{\infty} B_{1mn}\left(\frac{\mathrm{J}_1(\mu_n)}{\mu_n}\right)\left(\int_0^t \mathrm{e}^{-(\mu_m^2-\mu_n^2)s} D_{mn}(s)\,\mathrm{d}s\right)\mathrm{e}^{-\mu_n^2 t}}{\displaystyle\sum_{n=0}^{\infty} B_{2n}\left(\frac{\mathrm{J}_1(\mu_n)}{\mu_n}\right)\mathrm{e}^{-\mu_n^2 t}}, \tag{3.27}$$

$$D_{mn}(s) = \int_0^1 r w(s, r)\mathrm{J}_0(\mu_m r)\mathrm{J}_0(\mu_n r)\,\mathrm{d}r$$
$$= w_1(s)\int_0^{r_p} r\mathrm{J}_0(\mu_m r)\mathrm{J}_0(\mu_n r)\,\mathrm{d}r + \int_{r_p}^1 r w_2(s, r)\mathrm{J}_0(\mu_m r)\mathrm{J}_0(\mu_n r)\,\mathrm{d}r, \tag{3.28}$$

$$\left.\begin{aligned} &B_{1mn} = A_m A_n'^2, \quad B_{2n} = A_n A_n'^2\left(\frac{\mathrm{J}_0^2(\mu_n)+\mathrm{J}_1^2(\mu_n)}{2}\right), \\ &A_n = \frac{\left(\mu_n^2\displaystyle\int_0^1 rY(r)\mathrm{J}_0(\mu_n r)\,\mathrm{d}r\right)}{(\mu_n^2+\beta^2)\mathrm{J}_0^2(\mu_n)\displaystyle\int_0^1 rY(r)\,\mathrm{d}r}, \quad A_n'^2 = \frac{2\mu_n^2}{(\mu_n^2+\beta^2)\mathrm{J}_0^2(\mu_n)}, \end{aligned}\right\} \tag{3.29}$$

$m = 0, 1, 2, \ldots$, $n = 0, 1, 2, \ldots$, and μ_n are the roots of transcendental equation

$$\mu_n \mathrm{J}_1(\mu_n) = \beta \mathrm{J}_0(\mu_n), \quad n = 0, 1, 2, \ldots. \tag{3.30}$$

From (3.8), $K_1(t)$ is obtained and it is represented as

$$K_1(t) = 2\frac{\partial f_1}{\partial r}(t, 1) - 2\int_0^1 f_0(t, r) w(t, r) r\,\mathrm{d}r, \tag{3.31}$$

where

$$\frac{\partial f_1}{\partial r}(t, 1) = \frac{\displaystyle\sum_{n=0}^{\infty}\left[\sum_{m=0}^{\infty} B_{1mn}\left(\int_0^t \mathrm{e}^{-(\mu_m^2-\mu_n^2)s} D_{mn}(s)\,\mathrm{d}s\right) + B_{2n}F_1(t)\right]\mu_n \mathrm{J}_1(\mu_n)\mathrm{e}^{-\mu_n^2 t}}{2\displaystyle\sum_{n=0}^{\infty}(A_n/\mu_n)\mathrm{J}_1(\mu_n)\mathrm{e}^{-\mu_n^2 t}}. \tag{3.32}$$

Now from (3.31) using (3.20), (3.27)–(3.30) and (3.32), the convective coefficient $K_1(t)$ is obtained numerically using the Simpson's 1/3 rule for integration.

3.3. *Estimation of $f_2(t, r)$ and $K_2(t)$*

By taking $n = 2$ in (3.10), we obtain the equation for $f_2(t, r)$ involving the dispersion coefficient $K_2(t)$ as

$$\frac{\partial f_2}{\partial t} = \frac{1}{r}\frac{\partial}{\partial r}\left(r\frac{\partial f_2}{\partial r}\right) - f_2 K_0 + \left(\frac{1}{Pe^2} - K_2\right) f_0 - (w(t, r) + K_1) f_1. \tag{3.33}$$

https://doi.org/10.1017/jfm.2016.155 Published online by Cambridge University Press

The initial and boundary conditions are obtained from (3.13)–(3.15) for $n=2$, and the addition condition is given by

$$\int_0^1 f_2(t, r) r \, \mathrm{d}r = 0. \tag{3.34}$$

Using the method of eigenfunction expansion, the solution of (3.33) for $f_2(t, r)$ satisfying the initial and boundary conditions (3.13)–(3.15) and the additional condition (3.34) is obtained as

$$f_2(t, r) = \frac{\displaystyle\sum_{n=0}^{\infty} \left[\sum_{m=0}^{\infty} B_{3mn} \left(\sum_{k=0}^{\infty} F_{3mnk}(t) + F_{4mn}(t) \right) - B_{5n} F_2(t) + \sum_{m=0}^{\infty} B_{4n} F_{5mn}(t) \right] \mathrm{J}_0(\mu_n r) \mathrm{e}^{-\mu_n^2 t}}{2 \displaystyle\sum_{n=0}^{\infty} (A_n/\mu_n) \mathrm{J}_1(\mu_n) \mathrm{e}^{-\mu_n^2 t}}, \tag{3.35}$$

where

$$\begin{aligned} F_2(t) &= \int_0^t \left(K_2(s) - \frac{1}{Pe^2} \right) \mathrm{d}s \\ &= \frac{\displaystyle\sum_{n=0}^{\infty} \left[\sum_{m=0}^{\infty} B_{3mn} \left(\sum_{k=0}^{\infty} F_{3mnk}(t) + F_{4mn}(t) \right) + \sum_{m=0}^{\infty} B_{4n} F_{5mn}(t) \right] \left(\dfrac{\mathrm{J}_1(\mu_n)}{\mu_n} \right) \mathrm{e}^{-\mu_n^2 t}}{\displaystyle\sum_{n=0}^{\infty} B_{5n} \frac{\mathrm{J}_1(\mu_n)}{\mu_n} \mathrm{e}^{-\mu_n^2 t}}, \end{aligned} \tag{3.36}$$

$$F_{3mnk}(t) = A_k A'_m \int_0^t \left[\mathrm{e}^{-(\mu_m^2 - \mu_n^2)s} \left(\int_0^s \mathrm{e}^{-(\mu_k^2 - \mu_m^2)s'} D_{km}(s') \, \mathrm{d}s' \right) D_{mn}(s) \right] \mathrm{d}s, \tag{3.37}$$

$$F_{4mn}(t) = A_m A'_m \left(\frac{\mathrm{J}_0^2(\mu_m) + \mathrm{J}_1^2(\mu_m)}{2} \right) \int_0^t \mathrm{e}^{-(\mu_m^2 - \mu_n^2)s} \left[\left(\int_0^s K_1(s') \, \mathrm{d}s' \right) D_{mn}(s) \right] \mathrm{d}s, \tag{3.38}$$

$$F_{5mn}(t) = \int_0^t \left[\int_0^s \left(E_{mn}(s') + A_n A'_n \left(\frac{\mathrm{J}_0^2(\mu_n) + \mathrm{J}_1^2(\mu_n)}{2} \right) K_1(s') \right) \mathrm{d}s' \right] K_1(s) \, \mathrm{d}s, \tag{3.39}$$

$$E_{mn}(s') = A_m A'_n \mathrm{e}^{-(\mu_m^2 - \mu_n^2)s'} D_{mn}(s'), \tag{3.40}$$

$$\begin{aligned} D_{mn}(s) &= \int_0^1 r w(s, r) \mathrm{J}_0(\mu_m r) \mathrm{J}_0(\mu_n r) \, \mathrm{d}r \\ &= w_1(s) \int_0^{r_p} r \mathrm{J}_0(\mu_m r) \mathrm{J}_0(\mu_n r) \, \mathrm{d}r + \int_{r_p}^1 r w_2(s, r) \mathrm{J}_0(\mu_m r) \mathrm{J}_0(\mu_n r) \, \mathrm{d}r, \end{aligned} \tag{3.41}$$

https://doi.org/10.1017/jfm.2016.155 Published online by Cambridge University Press

$$\left.\begin{aligned} B_{3mn} &= A'_m A''_n, \quad B_{4n} = A'_n A''_n \left(\frac{\mathrm{J}_0^2(\mu_n) + \mathrm{J}_1^2(\mu_n)}{2}\right), \\ B_{5n} &= A_n A''_n \left(\frac{\mathrm{J}_0^2(\mu_n) + \mathrm{J}_1^2(\mu_n)}{2}\right), \quad A_n = \frac{\mu_n^2 \displaystyle\int_0^1 rY(r)\mathrm{J}_0(\mu_n r)\,\mathrm{d}r}{(\mu_n^2+\beta^2)\mathrm{J}_0^2(\mu_n)\displaystyle\int_0^1 rY(r)\,\mathrm{d}r}, \\ A'_n &= \frac{\sqrt{2}\mu_n}{\sqrt{(\mu_n^2+\beta^2)}\mathrm{J}_0(\mu_n)}, \quad A''^2_n = \frac{2\mu_n^2}{(\mu_n^2+\beta^2)\mathrm{J}_0^2(\mu_n)}, \end{aligned}\right\} \tag{3.42}$$

$m = 0, 1, 2, \ldots$, $n = 0, 1, 2, \ldots$, and μ_n are the roots of transcendental equation

$$\mu_n \mathrm{J}_1(\mu_n) = \beta \mathrm{J}_0(\mu_n), \quad n = 0, 1, 2, \ldots. \tag{3.43}$$

From (3.8), $K_2(t)$ is obtained as

$$K_2(t) = \frac{1}{Pe^2} + 2\frac{\partial f_2}{\partial r}(t, 1) - 2\int_0^1 f_1(t, r)w(t, r)r\,\mathrm{d}r, \tag{3.44}$$

where

$$\frac{\partial f_2}{\partial r}(t, 1) = -\frac{\displaystyle\sum_{n=0}^{\infty}\left[\sum_{m=0}^{\infty} B_{3mn}\left(\sum_{k=0}^{\infty} F_{3mnk}(t) + F_{4mn}(t)\right) - B_{5n}F_2(t) + \sum_{m=0}^{\infty} B_{4n}F_{5mn}(t)\right]F_{6n}(t)}{2\displaystyle\sum_{n=0}^{\infty}(A_n/\mu_n)\mathrm{J}_1(\mu_n)\mathrm{e}^{-\mu_n^2 t}} \tag{3.45}$$

and

$$F_{6n}(t) = \mu_n \mathrm{J}_1(\mu_n)\mathrm{e}^{-\mu_n^2 t}. \tag{3.46}$$

Now from (3.44) using (3.26), (3.36)–(3.43), (3.45) and (3.46), the dispersion coefficient $K_2(t)$ is obtained numerically using the Simpson's 1/3 rule of integration.

3.4. *Solution for mean concentration* $C_m(t, z)$

The solution of (3.7) satisfying the initial and boundary conditions (3.11), (3.16) is given by

$$C_m(t, z) = \frac{1}{2Pe\sqrt{\pi T}} \exp\left(\xi - \frac{z_1^2}{4T}\right), \tag{3.47}$$

where

$$\xi(t) = \int_0^t K_0(\eta)\,\mathrm{d}\eta, \tag{3.48a}$$

$$z_1(t, z) = z + \int_0^t K_1(\eta)\,\mathrm{d}\eta, \tag{3.48b}$$

and

$$T(t) = \int_0^t K_2(\eta)\,\mathrm{d}\eta. \tag{3.48c}$$

https://doi.org/10.1017/jfm.2016.155 Published online by Cambridge University Press

Vessel	Radius (cm)	α	References
Proximal aorta	1.5	21.7	Truskey *et al.* (2004)
Abdominal aorta	—	12.0	Bronzino (1999)
Left main coronary artery	0.425	6.15	Truskey *et al.* (2004)
Renal artery	—	4.0	Bronzino (1999)
Femoral artery	0.27	3.9	Truskey *et al.* (2004)
Left anterior descending coronary artery	0.17	2.4	Truskey *et al.* (2004)
Right coronary artery	0.097	1.82	Truskey *et al.* (2004)
Terminal arteries	0.05	0.72	Truskey *et al.* (2004)

TABLE 1. Values of Womersley frequency parameter α in human circulatory system.

4. Results and discussion

This study is undertaken to analyse the dispersion process of a solute in the pulsatile flow of Casson fluid through a tube with the irreversible boundary reaction. The generalized dispersion model suggested by Sankarasubramanian & Gill (1973) is applied to determine the three effective transport coefficients, i.e. the exchange, convection and dispersion coefficients which describe the whole dispersion process of solute. In the present analysis, the effect of wall absorption parameter β on these three coefficients, the effect of yield stress τ_y, the fluctuating pressure component e and Womersley frequency parameter α on the convection and dispersion coefficients is analysed by fixing the Schmidt number $Sc = 1000$ and Peclet number $Pe = 1000$. The Schmidt number Sc which is the ratio of viscous diffusion to molecular diffusion, is taken as $O(10^3)$ (Caro *et al.* 1978; Mazumder & Das 1992; Truskey, Yuan & Katz 2004) in arterial blood flows. In accordance with the physical process considered in the present investigations, the value of Peclet number Pe is considered as 1000 (Mazumder & Das 1992; Nagarani & Sebastian 2013). The variations in axial mean concentration C_m has been discussed with the effect of wall absorption, yield stress and flow pulsatility using the expressions given in (3.47) and (3.48*a–c*).

In this study, the value of β is taken in the range 0–100 to account for small and large absorption rates at the wall (Sankarasubramanian & Gill 1973; Nagarani *et al.* 2004). The experimental values of β are 0.7 for carbon dioxide, and $\beta \to \infty$ for acetaldehyde (Kaye, Kavafyan & Schroter 1993). By considering a small perturbation parameter ε $(= 1/Sc)$, the nonlinear coupled equations (2.22) and (2.23) are solved to analyse the velocity distribution of Casson fluid for both small and large values of the frequency parameter α. The parameter α is the ratio of unsteady inertial force to viscous force, and it can be rewritten as $R/\sqrt{(\nu/\omega)}$ or $\sqrt{2\pi}R/\sqrt{(\nu T)}$, where T is the period of pulsation. In the human circulatory system, α ranges from $O(10^{-3})$ in the capillaries to nearly 20 in the ascending aorta at rest (Caro *et al.* 1978; Chandran, Rittgers & Yoganathan 2012). The values of α in human arteries are given in table 1. In this analysis, α is taken as 0.05, 0.1, 0.2, 0.5, 1, 2, 3, 3.05, 4, 6 and 10 to compare the present results with those existing in the literature. Due to pulsatile nature of the pressure, the velocity of the fluid is periodic in time with period $2\pi/\alpha^2 Sc$ and hence for $\alpha = 0.05$, 0.1, 0.2, 0.5, 1, 2, 3, 3.05, 4, 6 and 10, the time periods are calculated as 2.513, 0.628, 0.157, 0.025, 0.00628, 0.00157, 0.000698, 0.000675, 0.00039, 0.0001745 and 0.0000628, respectively. All the results in the present investigations are shown for three cycles of oscillation. Since the fluctuating pressure component e varies from 0 to 1, its value is taken as 0.5 (Nagarani & Sebastian 2013) in this study. The value

https://doi.org/10.1017/jfm.2016.155 Published online by Cambridge University Press

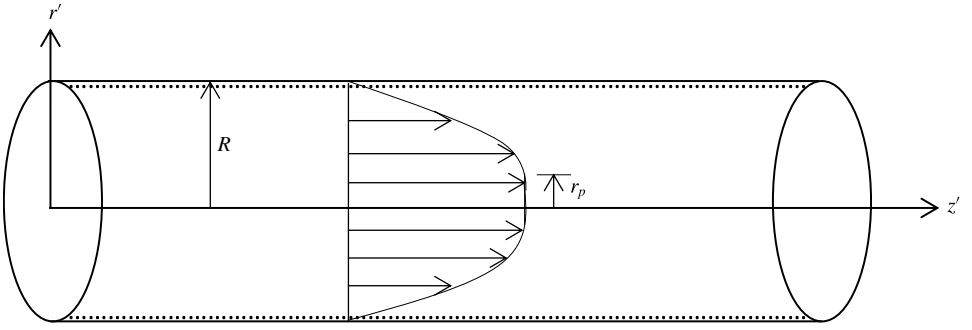


FIGURE 1. Schematic diagram of proposed model.

of yield stress τ_y in the range 0–0.1 is appropriate for physiological flow situations in blood vessels (Dash, Jayaraman & Mehta 1996). The value of τ_y is taken in the range 0–0.05 (Nagarani & Sebastian 2013). The value of the diffusion coefficient in blood varies in the range 0.75×10^{-5} to 0.5×10^{-5} cm^2 s^{-1} at a hematocrit of 33–45 % (Nagarani *et al.* 2004). When $e \to 0$, $\tau_y = 0$ and time is very large, the present results are found to be in agreement with Sankarasubramanian & Gill (1973) and Nagarani *et al.* (2004).

Integrals involved in the solution of convection coefficient $K_1(t)$, dispersion coefficient $K_2(t)$ and mean concentration $C_m(t, z)$ are evaluated numerically using Simpson's 1/3 rule. It is seen that the exchange coefficient $K_0(t)$ depends on wall absorption parameter β. The convection coefficient $K_1(t)$ and dispersion coefficient $K_2(t)$ depend on wall absorption parameter β, yield stress τ_y, fluctuating pressure component e of the fluid and Womersley frequency parameter α.

4.1. *Exchange coefficient* $K_0(t)$

The amount of solute is continuously reduced in the tube due to the irreversible first-order reaction occurring at the tube wall. From (3.15) for $n = 0$ and (3.23), it is seen that the exchange coefficient $K_0(t)$ directly depends on the wall absorption parameter β. The coefficient $K_0(t)$ accounting for the non-zero solute flux at the tube wall will be negative for the depletion of solute in the system. At the time $t = 0$, K_0 becomes zero due to the absence of solute at the tube wall. As the time increases, solute moves along the tube and diffuses to the wall region. Due to which, the concentration of solute increases at the wall region. An equilibrium between the diffusive transport from the centre of the tube to the wall region and the reaction at the wall occurs due to which there is a steady state of the process and from that instant, K_0 becomes constant. Figure 2 shows the variation of negative exchange coefficient $-K_0$ with time for $\beta = 0.01$, 1 and 100, respectively. From this figure, it is seen that there is no significant change in $-K_0$ with time t for $\beta = 0.01$ and $\beta = 1$. But the magnitude of $-K_0$ decreases rapidly as t increases for large values of β ($\beta = 100$ is shown in the figure 2) and after a certain time it reaches a constant value. For small values of β, an equilibrium between the diffusion of solute and the wall reaction occurs within small time and K_0 reaches the constant value. But, for large β, as the time increases, solute in the system is reduced more rapidly due to the reaction at the wall and large time is taken to reach a steady state. From figure 2, it is also seen that as β increases, $-K_0$ increases at initial time. The same phenomenon for $-K_0$ was reported for $\beta = 0.01$, 1 and 100 by Sankarasubramanian & Gill (1973).

https://doi.org/10.1017/jfm.2016.155 Published online by Cambridge University Press

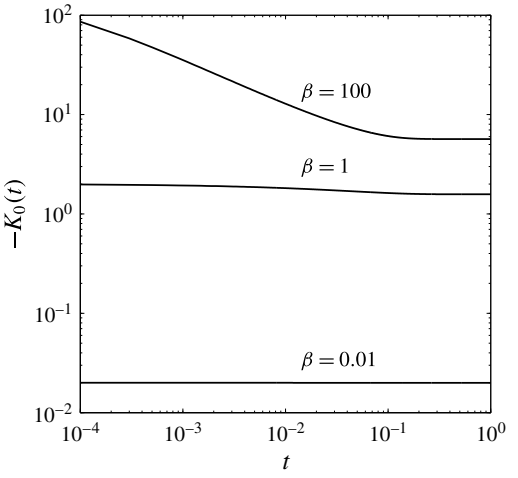


FIGURE 2. Variation of negative exchange coefficient $-K_0(t)$ with time for wall absorption parameter $\beta = 0.01,\ 1$ and 100.

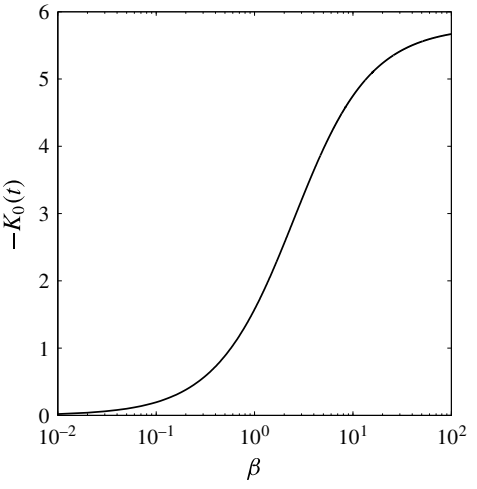


FIGURE 3. Variation of negative exchange coefficient $-K_0(t)$ at large time $t = 1$ with wall absorption parameter β.

Figure 3 shows the variation of negative exchange coefficient $-K_0$ with β at large time t (Here the time $t = 1$ is taken as very large). As β increases, the magnitude of $-K_0$ increases continuously and becomes 5.669 at $t = 1$ for $\beta = 100$. Further, for very large values of β, it approaches the value 5.78, as discussed in Sankarasubramanian & Gill (1973). The reason for this is because at sufficiently large value of β, solute is consumed rapidly by the first-order reaction at the wall than it is supplied by the molecular diffusion and as a result the diffusion process is stabilized. It is worth mentioning that the exchange coefficient $K_0(t)$ is independent of the nature of the fluid (Newtonian/non-Newtonian) and the pulsatility of the vessels. Hence, the coefficient $K_0(t)$ is independent of τ_y, e and α.

https://doi.org/10.1017/jfm.2016.155 Published online by Cambridge University Press

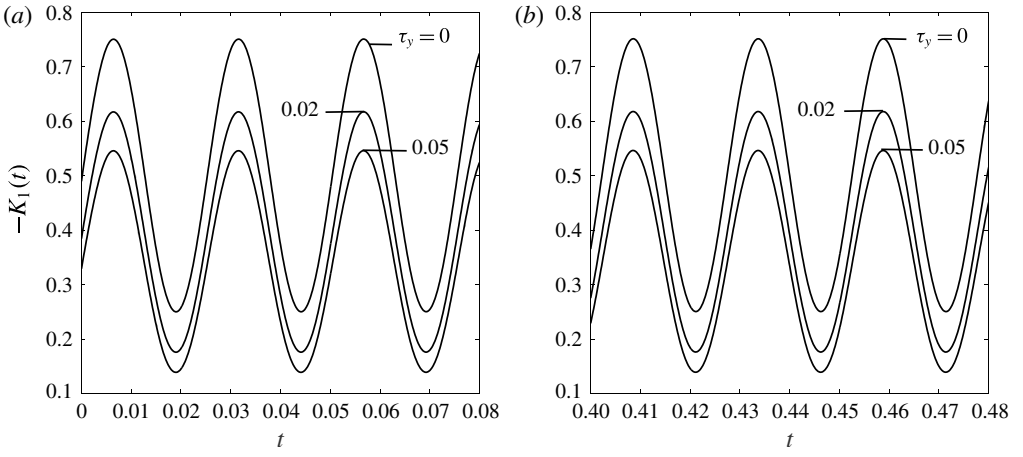


FIGURE 4. Variation of negative convection coefficient $-K_1(t)$ with t for different values of τ_y when $\beta = 0.01$, $\alpha = 0.5$, $e = 0.5$ and $Sc = 1000$. (*a*) For small times; (*b*) for large times.

4.2. *Convection coefficient* $K_1(t)$

The convective coefficient K_1 is arising because of the fluid movement, unlike K_0, the convection coefficient depends on yield stress of the fluid τ_y, amplitude of the fluctuating pressure component e and frequency parameter α. In this analysis, the effects of τ_y, e, β and α on negative convection coefficient $-K_1$ have been discussed for small and large time.

The variation of negative convection coefficient $-K_1$ with small and large time for different values of yield stress τ_y has been shown in figure 4(*a*,*b*). From these figures, it is seen that as τ_y increases, both the amplitude of fluctuations and the magnitude of $-K_1$ decreases. The coefficient $-K_1$ oscillates and reaches a non-transient state after certain period of time. For yield stress $\tau_y = 0$, 0.02 and 0.05, $-K_1$ starts to oscillate at initial time $t = 0$ from the values 0.49, 0.384 and 0.329, respectively. So, solute is started initially to convect with the velocity of the fluid 0.49 along the tube for $\tau_y = 0$. At non-transient state in each period of oscillation, $-K_1$ reaches a constant value 0.74, 0.62 and 0.549 for $\tau_y = 0$, 0.02 and 0.05, respectively. Due to increase in τ_y or in other words, increase in the non-Newtonian parameter decreases the velocity of the fluid, which in turn caused a reduction in the value of $-K_1$.

Figure 5(*a*,*b*) show the variation of $-K_1$ with small and large time for different values of fluctuating pressure component e. It is observed from these figures that the amplitude of fluctuations of $-K_1$ increases with e. The flow is steady for the case $e = 0$. In steady flow at non-transient state, $-K_1$ reaches a constant value 0.336, that means the solute is convected along the tube with the constant velocity of the fluid 0.336 for $\tau_y = 0.05$. For unsteady flow at non-transient state, the amplitude of fluctuations of $-K_1$ reaches a constant value 0.549 and 0.421 in each cycle of oscillation when $e = 0.5$ and $e = 0.2$, respectively. The critical time for which K_1 reaches a non-transient state is independent of e. As e increases, fluctuating component of the pressure gradient increases and hence flow velocity increases which leads to increase in $-K_1$.

The variation of $-K_1$ has been shown at small and large time for different values of wall absorption parameter β in figure 6. For $\beta = 0.01$, the fluctuation of $-K_1$ does

https://doi.org/10.1017/jfm.2016.155 Published online by Cambridge University Press

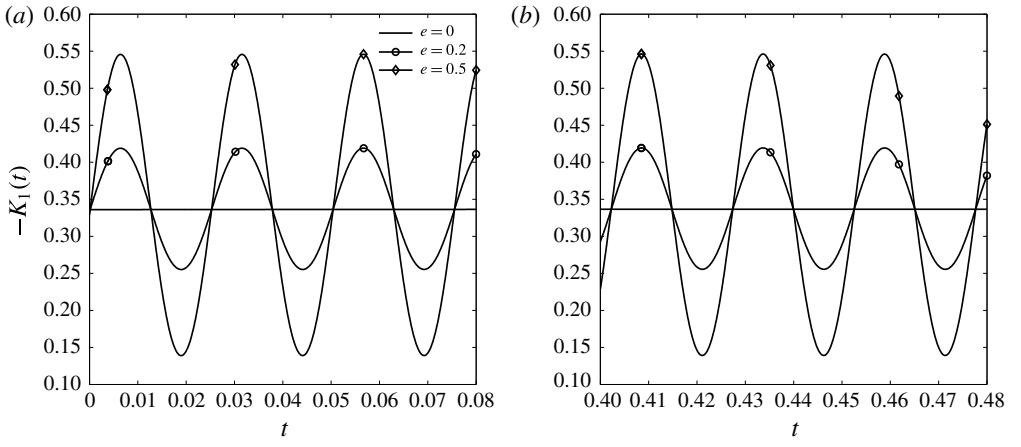


FIGURE 5. Variation of negative convection coefficient $-K_1(t)$ with t for different values of e when $\tau_y = 0.05$, $\beta = 0.01$, $\alpha = 0.5$ and $Sc = 1000$. (*a*) For small times; (*b*) for large times.

not increase significantly and reaches a stationary state at small time after certain period of oscillation. But for $\beta = 1$ and $\beta = 100$, the amplitude of oscillations of $-K_1$ increases at small time and becomes stable at large time. At each period of oscillation in stationary state, $-K_1$ reaches a constant value 0.809, 0.61 and 0.549 for $\beta = 100$, 1 and 0.01, respectively. It is evident from these figures that as β increases, the amplitude of oscillations of $-K_1$ increases at small and large time. The growth of oscillations of $-K_1$ at small time becomes larger for larger values of β. The reason for this enhancement of $-K_1$ at large value of β is due to the consumption of solute in the presence of boundary absorption at the wall. Higher values of β satisfies more absorption at the wall region and lesser solute is available for convection compared to that at the central region of the tube. So, the solute distribution is weighted in favour of the central region and solute is convected with faster velocity near the central region than that at the wall region. From the figures 7–9, it is also seen that as β increases, the amplitude of oscillations of $-K_1$ increases for different values of α. But the difference between the amplitude of fluctuations of $-K_1$ for different values of β decreases as α increases and becomes very small at large value of α.

The Womersley frequency parameter α is seen to have significant influence on $-K_1$ in the case of non-Newtonian fluid. Figures 6–9 show the variation of $-K_1$ with small and large time for different values of $\alpha = 0.5$, 1, 4 and 10. It can be observed that the amplitude of fluctuation of $-K_1$ increases with α. The period of oscillation becomes short at large value of α. At small time, the fluctuation of $-K_1$ does not increase significantly for large values of α and $-K_1$ reaches a stationary state at small time. In each period of oscillation for $\beta = 0.01$, $-K_1$ reaches a constant value 0.549, 0.551, 0.845 and 3.195 at non-transient state for $\alpha = 0.5$, 1, 4 and 10, respectively. It also seen that as α increases, the magnitude of $-K_1$ decreases initially at time $t = 0$ but after that the amplitude of fluctuations of $-K_1$ increases more and becomes positive and negative during the period of oscillation. The negative value of $-K_1$ occurs due to the flow reversal in the period.

When $e = 0$ and time t is very large, the variation of negative convection coefficient $-K_1$ with β for various values of the non-Newtonian parameter τ_y has been shown in

https://doi.org/10.1017/jfm.2016.155 Published online by Cambridge University Press

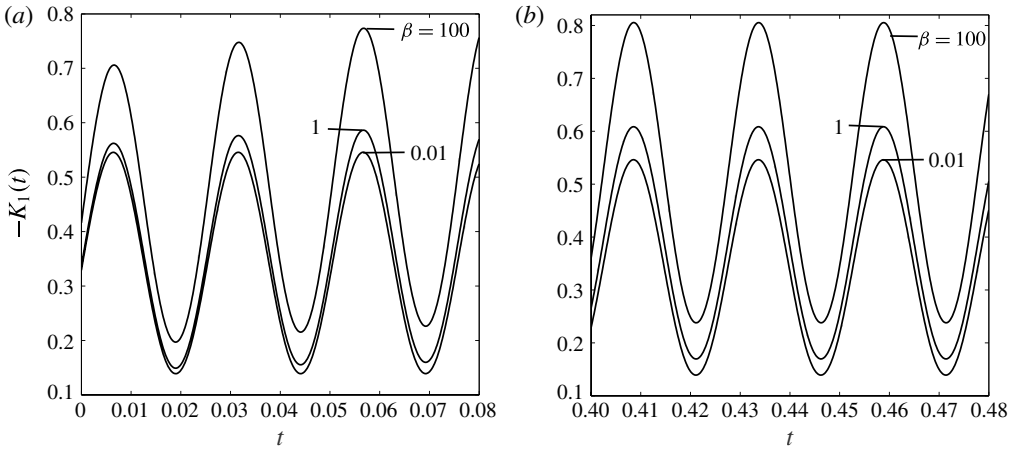


FIGURE 6. Variation of negative convection coefficient $-K_1(t)$ with t for different values of β when $\tau_y = 0.05$, $\alpha = 0.5$, $e = 0.5$ and $Sc = 1000$. (*a*) For small times; (*b*) for large times.

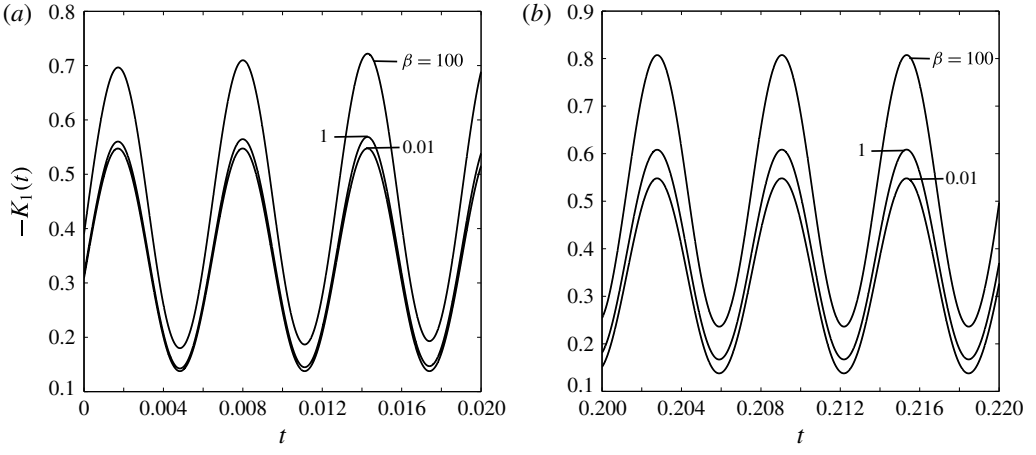


FIGURE 7. Variation of negative convection coefficient $-K_1(t)$ with t for different values of β when $\tau_y = 0.05$, $\alpha = 1$, $e = 0.5$ and $Sc = 1000$. (*a*) For small times; (*b*) for large times.

figure 10. It is observed that as β increases, the magnitude of $-K_1$ increases and it decreases as τ_y increases (Nagarani *et al.* 2004). The fluid velocity in Casson fluid is less compared to that of the Newtonian fluid and this leads to lesser convective coefficient in the Casson fluid. As $\beta \to \infty$, $K_1 \to -0.78$ for $\tau_y = 0$, i.e. as β increases, the coefficient $-K_1$ increases and possesses to the value 0.78 for $\tau_y = 0$. In the absence of wall absorption, i.e. for $\beta = 0$, the value of $-K_1$ is 0.5 which means that solute is moved along the tube with the average velocity of the flow. As β increases, solute is transported with the velocity higher than the average velocity of the flow. Similar profile for $-K_1$ with $\tau_y = 0$ is seen in Sankarasubramanian & Gill (1973) and Nagarani *et al.* (2004).

https://doi.org/10.1017/jfm.2016.155 Published online by Cambridge University Press

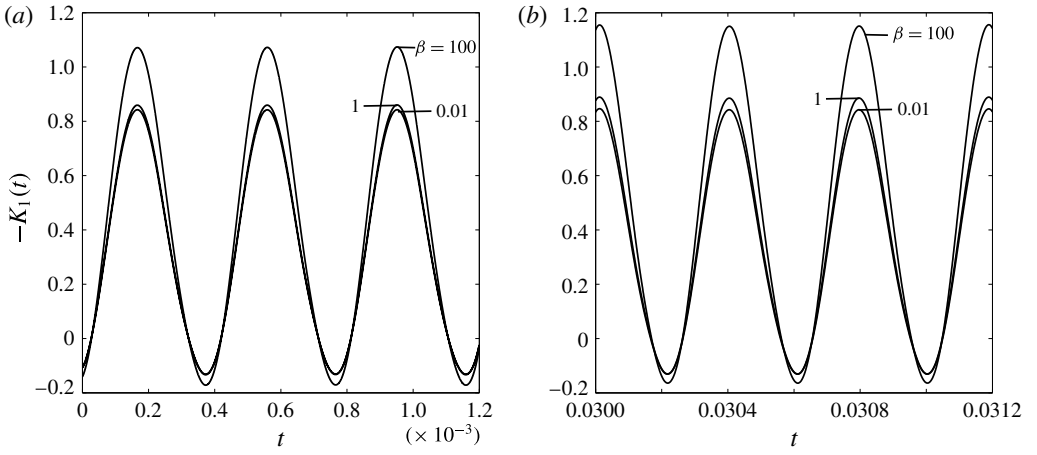


FIGURE 8. Variation of negative convection coefficient $-K_1(t)$ with t for different values of β when $\tau_y = 0.05$, $\alpha = 4$, $e = 0.5$ and $Sc = 1000$. (*a*) For small times; (*b*) for large times.

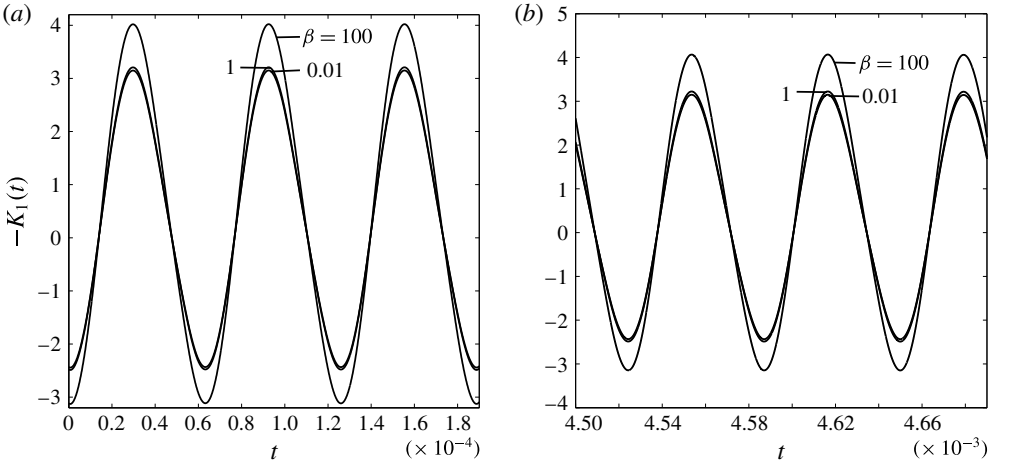


FIGURE 9. Variation of negative convection coefficient $-K_1(t)$ with t for different values of β when $\tau_y = 0.05$, $\alpha = 10$, $e = 0.5$ and $Sc = 1000$. (*a*) For small times; (*b*) for large times.

4.3. *Dispersion coefficient* $K_2(t)$

The dispersion coefficient K_2 depends on the yield stress of the fluid τ_y, amplitude of the fluctuating pressure component e, wall absorption parameter β and frequency parameter α. In the present study, the effects of τ_y, e, β and α on solute dispersion have been discussed for small as well as large time.

Figure 11(*a*,*b*) show the variation of dispersion coefficient K_2 (from which the additive contribution of the axial diffusion $1/Pe^2$ is deducted) with small and large time for different values of τ_y. From these figures, it is noticeable that as τ_y increases, both the amplitude of fluctuations and the magnitude of K_2 decreases. With the injection of solute in the blood flow, the solute dispersion starts within small time.

https://doi.org/10.1017/jfm.2016.155 Published online by Cambridge University Press

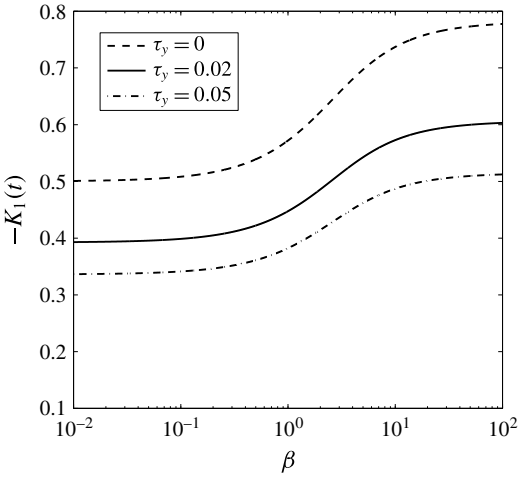


FIGURE 10. Variation of negative convection coefficient $-K_1(t)$ for different values of τ_y with wall absorption parameter β at large time $t = 1$ when $e = 0$.

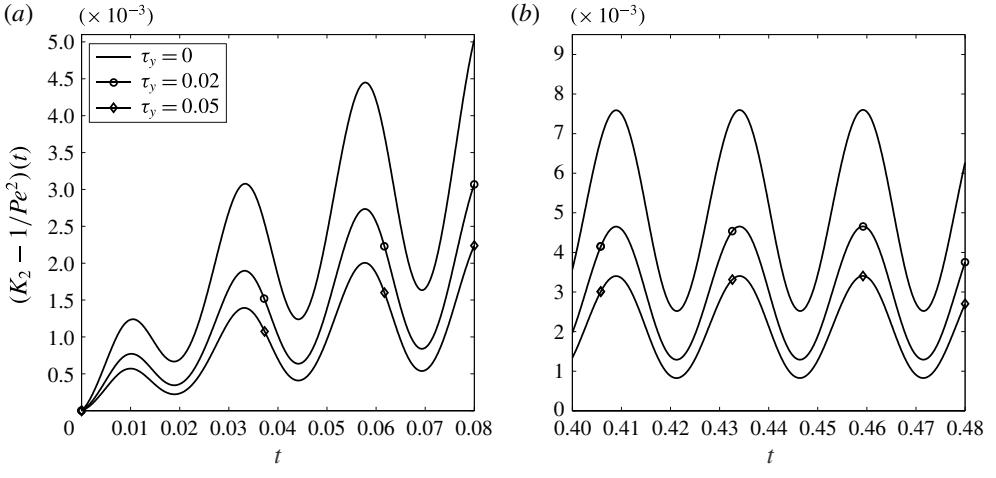


FIGURE 11. Variation of dispersion coefficient $(K_2 - 1/Pe^2)(t)$ with t for different values of τ_y when $\beta = 0.01$, $\alpha = 0.5$, $e = 0.5$ and $Sc = 1000$. (*a*) For small times; (*b*) for large times.

At small time, K_2 increases periodically with wavy nature and thereafter decreases as time increases and reaches a non-transient state at large time t, which is related to the characteristic time of transverse diffusion R^2/D_m. After the initial increment of the amplitude of oscillation for small time as seen in figure 11(*a*), these oscillations become stable at large time as large as $t \geqslant 0.4$ (as shown in figure 11*b*) and thereafter the dispersion of solute takes place with the period of oscillation at a uniform rate. Due to increase in τ_y, the velocity decreases and hence a decrease in the dispersion coefficient is noticed.

In figure 12(*a*,*b*), the variation of dispersion coefficient K_2 at all times is shown for steady flow ($e = 0$) of Newtonian fluid ($\tau_y = 0$) and Casson fluid ($\tau_y = 0.05$) with and

https://doi.org/10.1017/jfm.2016.155 Published online by Cambridge University Press

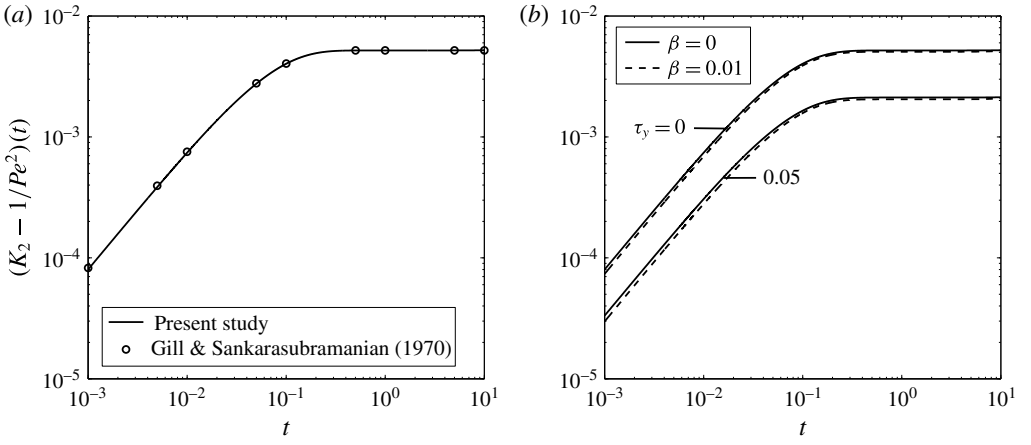


FIGURE 12. Variation of dispersion coefficient $(K_2 - 1/Pe^2)(t)$ with t for different values of τ_y and β at small and large time when $e = 0$. The data of Gill & Sankarasubramanian (1970) for K_2 is obtained from the equations (19) and (20) of their paper. (*a*) $\tau_y = 0$ with $\beta = 0$; (*b*) $\tau_y = 0$ and 0.05 with $\beta = 0$ and 0.01.

without the effect of wall absorption ($\beta = 0.01$ and $\beta = 0$). Present result (shown in the figure 12*a*) for steady flow of Newtonian fluid in the absence of wall absorption matches exactly with the result of Gill & Sankarasubramanian (1970) (figure 1) at small and large time. Also, our result for steady flow of Newtonian fluid with the effect of wall absorption is found to be in best agreement with Sankarasubramanian & Gill (1973) at very large time. From figure 12(*a*,*b*), it is seen that as time increases, K_2 increases rapidly at small time and reaches a constant value at large time ($t \geqslant 0.5$). For $\tau_y = 0$ and $\tau_y = 0.05$ with $\beta = 0$, K_2 reaches a constant value 5.21×10^{-3} and 2.13×10^{-3}, respectively at large time ($t \geqslant 0.5$). It is also observed that K_2 decreases as τ_y increases at small as well as large time. Also, K_2 decreases with the increment of wall absorption parameter β. But the difference of K_2 between the case of $\beta = 0$ and $\beta = 0.01$ is small and for each case K_2 attains a same constant value at very large time ($t = 10$).

At small as well as large time, the variation of K_2 for different values of e and τ_y has been presented for $\beta = 0$ and $\beta = 0.01$ in figures 13 and 14, respectively. For the clarity in comparison, these results are presented here for four cycles of oscillation for both Newtonian fluid ($\tau_y = 0$) and Casson fluid ($\tau_y = 0.05$). From these figures, it is seen that as e increases, both the amplitude of fluctuations and the magnitude of K_2 increases. For the steady flow, K_2 increases at small time and attains a value 4.04×10^{-3} at $t = 0.1$ and 5.19×10^{-3} at $t = 0.4$ for $\beta = 0$ and $\tau_y = 0$. For $\tau_y = 0$ with $\beta = 0.01$, K_2 reaches a value 3.89×10^{-3} at $t = 0.1$ and 5.04×10^{-3} at $t = 0.4$. For the unsteady flow ($e > 0$), K_2 increases cyclically at small time and reaches a stationary state at large time. At each cycle of oscillation in large time with $\tau_y = 0$ and $\beta = 0.01$, K_2 reaches a constant value 6.1×10^{-3} and 7.64×10^{-3} for $e = 0.2$ and $e = 0.5$, respectively. A similar nature is seen for other values of τ_y. The critical time at which K_2 reaches a non-transient state becomes independent of e. It is worth noting that the value of K_2 at small time $t = 0.1$ for steady flow of Newtonian fluid without wall absorption as observed by Nagarani & Sebastian (2013) (referred to their figure 5) is near about 1×10^{-3} which deviates much from the value (4.04×10^{-3}) of Gill & Sankarasubramanian (1970) (equations (19) and (20) therein, for K_2).

https://doi.org/10.1017/jfm.2016.155 Published online by Cambridge University Press

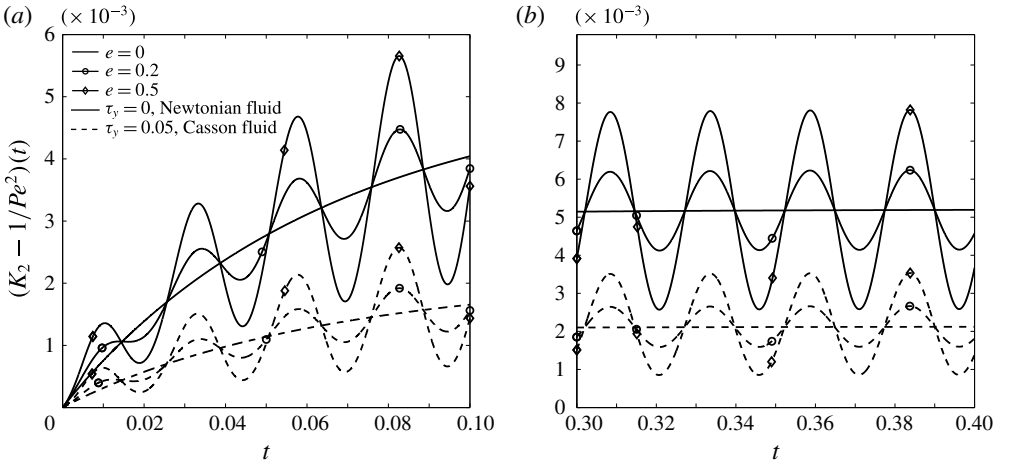


FIGURE 13. Variation of dispersion coefficient $(K_2 - 1/Pe^2)(t)$ with t for different values of e and τ_y when $\beta = 0$. (*a*) For small times; (*b*) for large times.

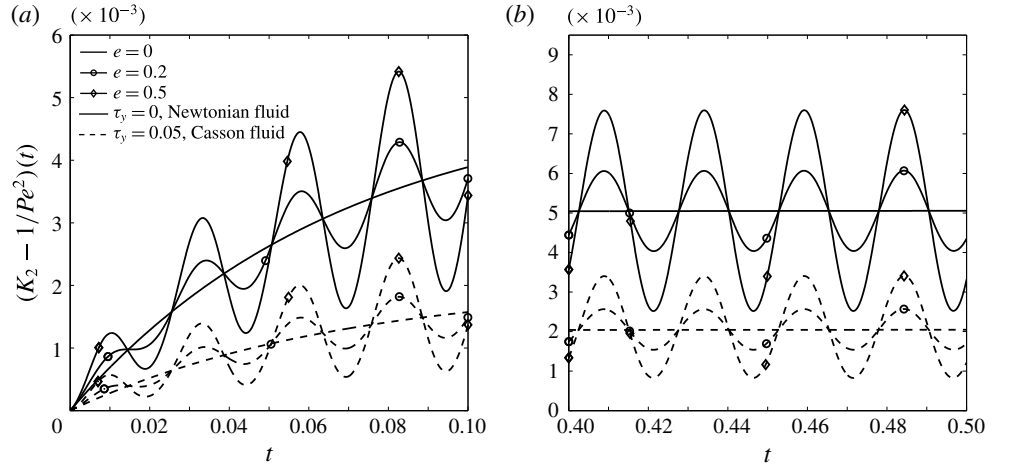


FIGURE 14. Variation of dispersion coefficient $(K_2 - 1/Pe^2)(t)$ with t for different values of e and τ_y when $\beta = 0.01$. (*a*) For small times; (*b*) for large times.

The effect on K_2 has been studied for different values of absorption parameter $\beta = 0$, 0.01, 1 and 100 with small and large time and it is shown in figures 15(*a*) and 15(*b*), respectively. It is observed from these figures that as β increases, both the amplitude of fluctuations and the magnitude of K_2 decreases. Initially, the amplitude of oscillation of K_2 increases and reaches a constant value 3.56×10^{-3}, 3.42×10^{-3}, 3.2×10^{-3} and 0.81×10^{-3} at each period of oscillation in large time for $\beta = 0$, 0.01, 1 and 100, respectively. With increase in the value of β, the dispersion coefficient K_2 decreases because number of moles of reactive material at the wall increases to undergo the chemical reaction or absorption and hence, more amount of solute near the wall is continuously depleted in the system. Therefore, the solute distribution is weighted in favour of the region near the centre of the tube and in this region, the solute is convected with the faster velocity than that near the wall region. So, the

https://doi.org/10.1017/jfm.2016.155 Published online by Cambridge University Press

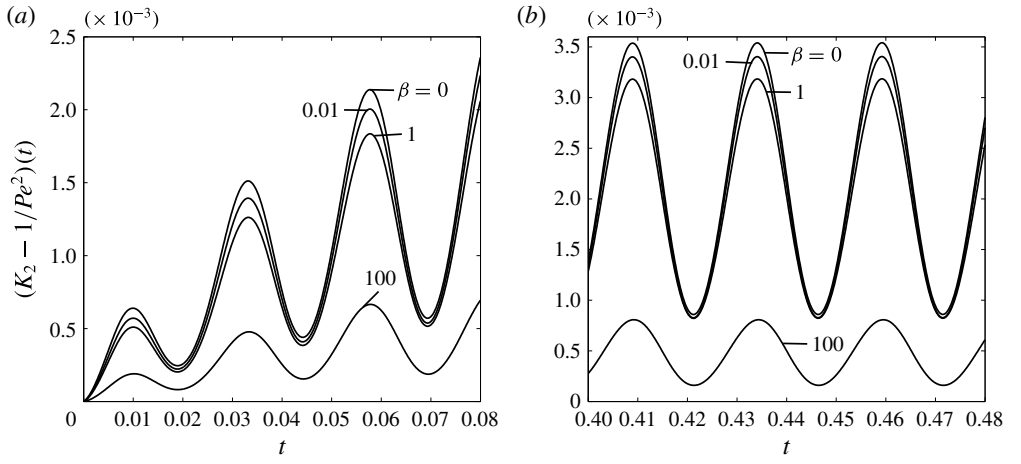


FIGURE 15. Variation of dispersion coefficient $(K_2 - 1/Pe^2)(t)$ with t for different values of β when $\tau_y = 0.05$, $\alpha = 0.5$, $e = 0.5$ and $Sc = 1000$. (*a*) For small times; (*b*) for large times.

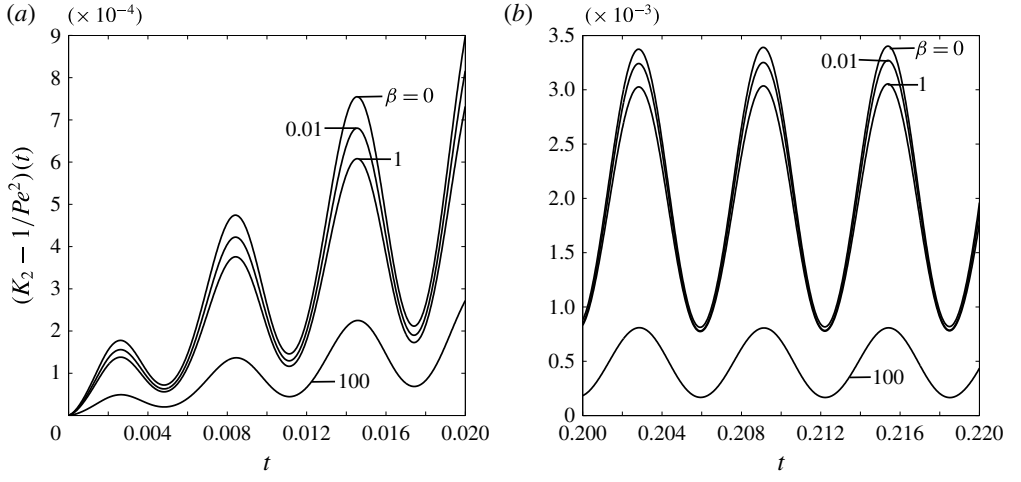


FIGURE 16. Variation of dispersion coefficient $(K_2 - 1/Pe^2)(t)$ with t for different values of β when $\tau_y = 0.05$, $\alpha = 1$, $e = 0.5$ and $Sc = 1000$. (*a*) For small times; (*b*) for large times.

velocity gradients are smaller near the central region than near the wall and smaller gradients cause smaller dispersion. This could be a reason for decrease in axial dispersion when β increases. Also, transverse diffusion of solute is increased by the larger transverse concentration gradients in the system with the presence of wall absorption and this causes the decrement in axial dispersion. From figures 16, 17 and 20–25, it is also noticed that the increase in β tends to decrease the axial dispersion for various values of α.

Variation of K_2 for small and large values of Womersley frequency parameter α is shown through the figures 15–17 and 22–25 for small and large time. From these figures, it is seen that as α increases, the axial dispersion decreases. The amplitude

https://doi.org/10.1017/jfm.2016.155 Published online by Cambridge University Press

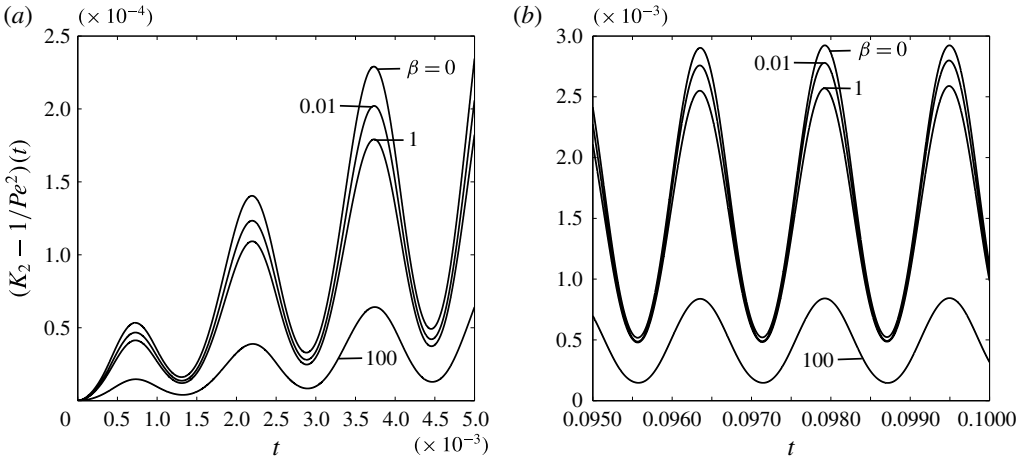


FIGURE 17. Variation of dispersion coefficient $(K_2 - 1/Pe^2)(t)$ with t for different values of β when $\tau_y = 0.05$, $\alpha = 2$, $e = 0.5$ and $Sc = 1000$. (*a*) For small times; (*b*) for large times.

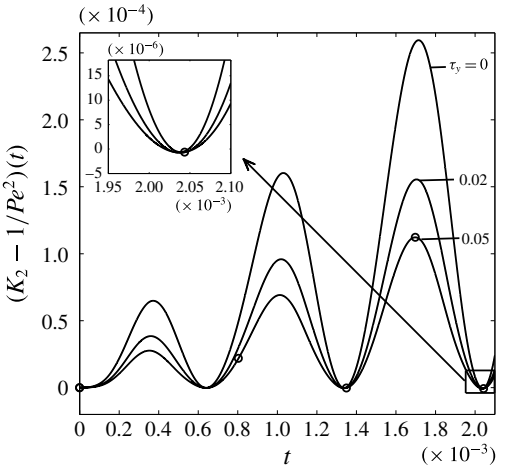


FIGURE 18. Variation of dispersion coefficient $(K_2 - 1/Pe^2)(t)$ with small time t for different values of τ_y when $\beta = 0.01$, $\alpha = 3$, $e = 0.5$ and $Sc = 1000$.

of fluctuations of K_2 decreases at both small and large time as α increases. For all values of α, K_2 oscillates in increasing manner at small time and reaches a static state in oscillation at large time. In each period of oscillation for $\beta = 0.01$, the dispersion coefficient becomes stable at large time with a constant value 5×10^{-3}, 3.42×10^{-3}, 3.28×10^{-3}, 2.8×10^{-3}, 2.1×10^{-3}, 1.75×10^{-3} and 1.5×10^{-3} for $\alpha = 0.1$, 0.5, 1, 2, 4, 6 and 10, respectively. As α increases, amplitude of oscillations of K_2 decreases and K_2 becomes negative during the period of oscillation for large values of α. This nature also depends on τ_y, e and β. From the figures 18 and 19, it is seen that K_2 attains the negative value within three cycles of oscillation in small time at $\alpha = 3$ for different values of τ_y and as τ_y increases, the peak of negative dispersion increases for a value of α around $\alpha = 3$. With $\alpha = 3.05$, this phenomenon is shown in figure 19.

https://doi.org/10.1017/jfm.2016.155 Published online by Cambridge University Press

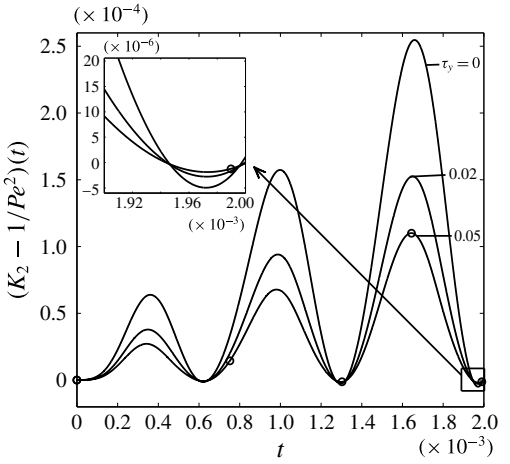


FIGURE 19. Variation of dispersion coefficient $(K_2 - 1/Pe^2)(t)$ with small time t for different values of τ_y when $\beta = 0.01$, $\alpha = 3.05$, $e = 0.5$ and $Sc = 1000$.

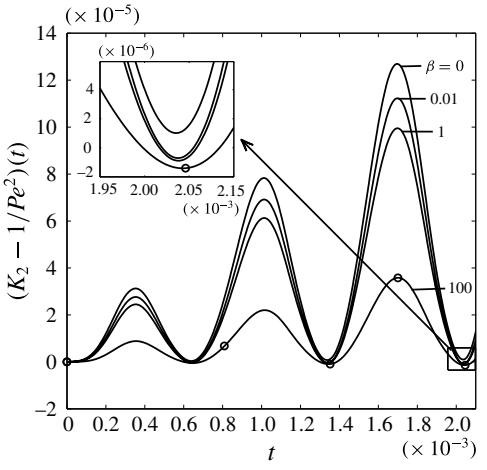


FIGURE 20. Variation of dispersion coefficient $(K_2 - 1/Pe^2)(t)$ with small time t for different values of β when $\tau_y = 0.05$, $\alpha = 3$, $e = 0.5$ and $Sc = 1000$.

Similar observations w.r.t. β are shown in figures 20 and 21. From these figures, it is observed that for $\beta = 0.01$, 1 and 100, K_2 becomes negative at $\alpha = 3$ but for $\beta = 0$, K_2 becomes negative at $\alpha = 3.05$ within three cycles of oscillation in small time. So, negative dispersion is seen at $\alpha = 3$ and the peak of negative dispersion increases with α. Womersley parameter directly depends on the radius of the vessel and its value is high in large vessels. The reversal of blood flow occurs in large vessels undergoing peristalsis (Craciunescu & Clegg 2001). The backward flow is experienced during late systole and early diastole in the arteries such as carotid, brachial, femoral arteries, renal arteries and abdominal aorta in which the values of α are large (Ku 1997). Due to the flow reversal in period, negative dispersion occurs and the material is moved back with the flow during the cycle of oscillation for large values of α (Mazumder

https://doi.org/10.1017/jfm.2016.155 Published online by Cambridge University Press

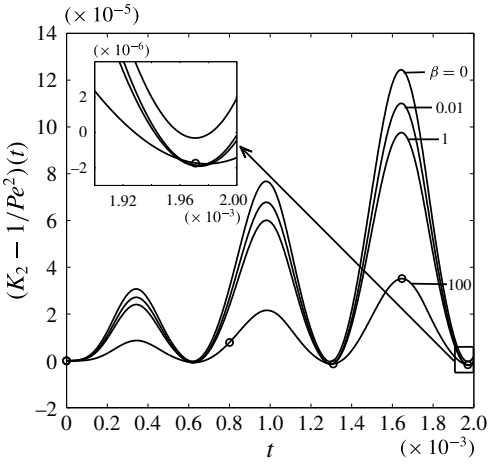


FIGURE 21. Variation of dispersion coefficient $(K_2 - 1/Pe^2)(t)$ with small time t for different values of β when $\tau_y = 0.05$, $\alpha = 3.05$, $e = 0.5$ and $Sc = 1000$.

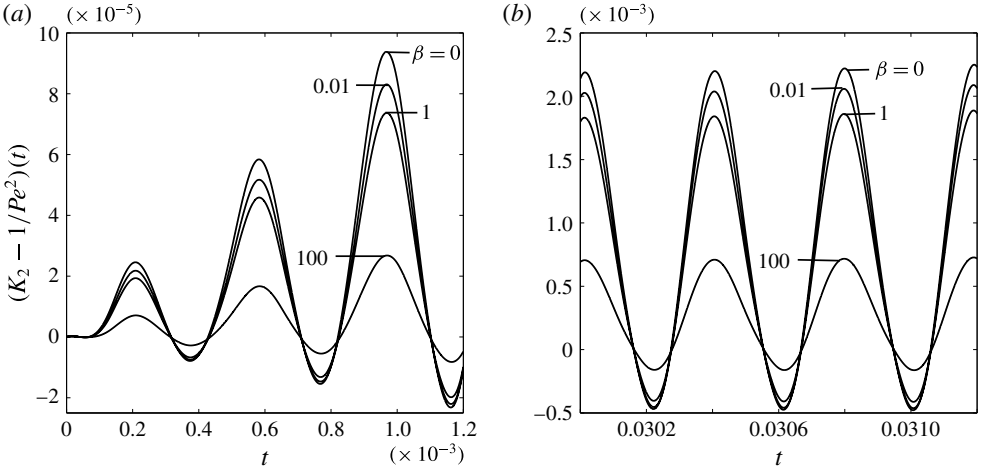


FIGURE 22. Variation of dispersion coefficient $(K_2 - 1/Pe^2)(t)$ with t for different values of β when $\tau_y = 0.05$, $\alpha = 4$, $e = 0.5$ and $Sc = 1000$. (*a*) For small times; (*b*) for large times.

& Das 1992). During the period of oscillation at each reversal of flow, the material dispersion is contracted (Smith 1982).

From figures 15–17, it can be seen that fluctuation of K_2 increases cyclically in small time with single frequency at each cycle of oscillation for $\alpha = 0.5$, 1 and 2. But, from the figures 23 and 24, it is observed that in small time, the amplitude of fluctuations of K_2 increases periodically with double frequency at first cycle for $\alpha = 6$ and at first two cycles of oscillation for $\alpha = 10$. The double frequency period was also observed by Mazumder & Das (1992) for Newtonian fluid. For $\alpha = 4$, very small double frequency period is seen in small time at first cycle of oscillation (see figure 22). So, double frequency period can be seen in the oscillation of K_2 at small time for large values of α ($\geqslant 4$) and becomes more frequent with the increase in α.

https://doi.org/10.1017/jfm.2016.155 Published online by Cambridge University Press

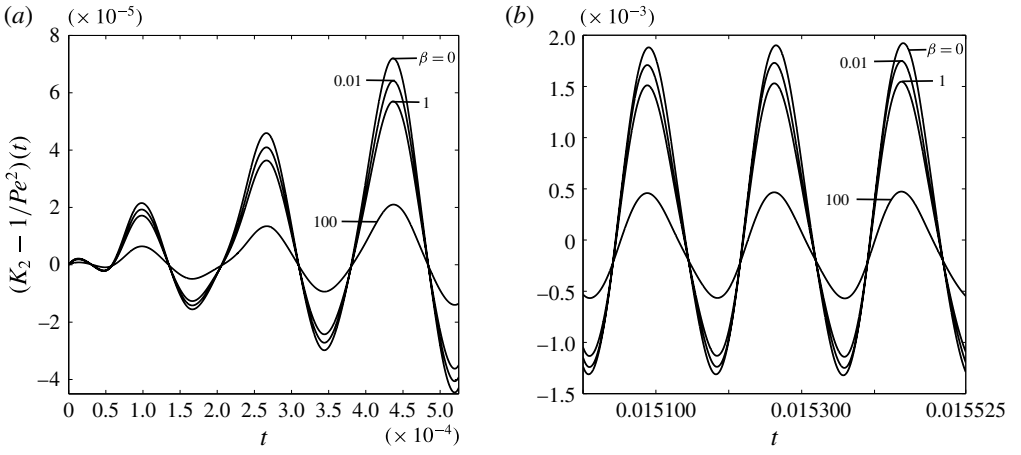


FIGURE 23. Variation of dispersion coefficient $(K_2 - 1/Pe^2)(t)$ with t for different values of β when $\tau_y = 0.05$, $\alpha = 6$, $e = 0.5$ and $Sc = 1000$. (a) For small times; (b) for large times.

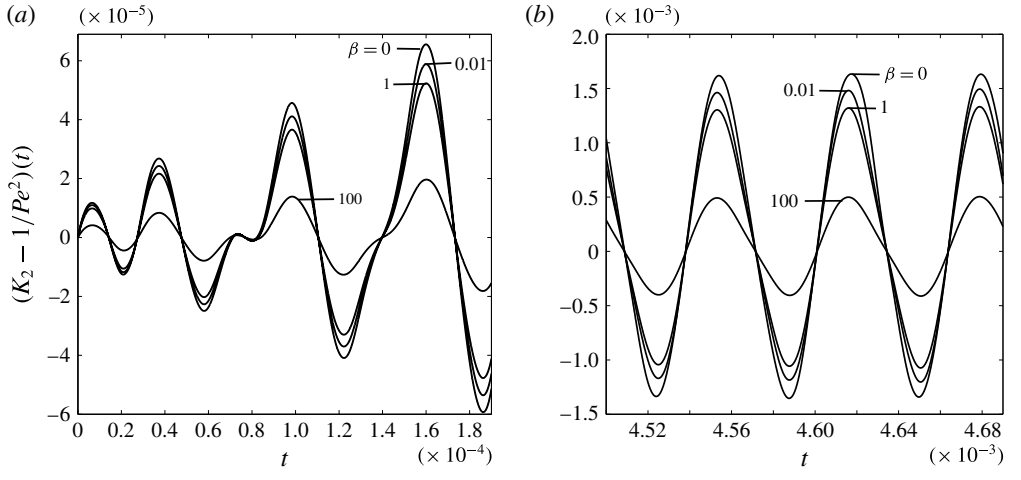


FIGURE 24. Variation of dispersion coefficient $(K_2 - 1/Pe^2)(t)$ with t for different values of β when $\tau_y = 0.05$, $\alpha = 10$, $e = 0.5$ and $Sc = 1000$. (a) For small times; (b) for large times.

From the figures 15–25, it is noticed that as α increases, the period of oscillations become shorter and the critical time for K_2 to reach a stationary state decreases.

From the figures 22 and 26, it is evident that for $\alpha = 4$, K_2 becomes both positive and negative during the period of oscillation. It is worth mentioning that Nagarani & Sebastian (2013) have not been able to notice this in their study, (see the figure 4 of Nagarani & Sebastian (2013)). This could be due to the error associated with the numerical integration of their equation (32) for finding K_2. This figure is reproduced in this work for the same set of parameter values and is shown in figure 26. Also, the expression given for K_1 is erroneous. In fact, the perturbation solution that was presented in Nagarani & Sebastian (2013) is valid only for small values of the

https://doi.org/10.1017/jfm.2016.155 Published online by Cambridge University Press

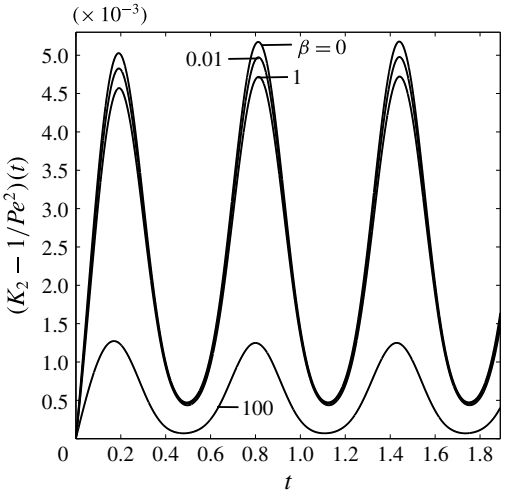


FIGURE 25. Variation of dispersion coefficient $(K_2 - 1/Pe^2)(t)$ with t for different values of β in small and large time when $\tau_y = 0.05$, $\alpha = 0.1$, $e = 0.5$ and $Sc = 1000$.

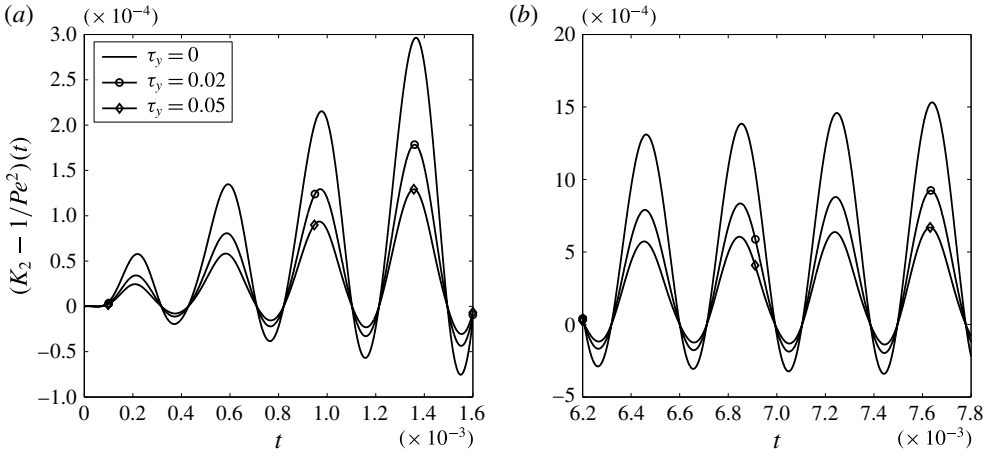


FIGURE 26. Variation of dispersion coefficient $(K_2 - 1/Pe^2)(t)$ with t for different values of τ_y when $\beta = 0$, $\alpha = 4$, $e = 0.5$ and $Sc = 1000$. (*a*) For small times; (*b*) for large times.

Womersley frequency parameter $\alpha < 1$, but they have considered the values as large as 4, which is not acceptable.

Limiting to smaller values of Womersley frequency parameter $\alpha < 1$, Sebastian & Nagarani (2015) studied the effect of wall absorption on the solute dispersion in pulsatile Casson fluid flow numerically using the Crank–Nicolson method adopted at each time step. The present investigation is a thorough analytical study considering the small and large values of Womersley frequency parameter α along with the effects of τ_y, e and β on both the convective coefficient K_1 and the dispersion coefficient K_2 and the present results are discussed already earlier in this paper. By considering the same set of parameters, we have re-examined the results that were presented in Sebastian & Nagarani (2015). Our results for small values of α are shown in

https://doi.org/10.1017/jfm.2016.155 Published online by Cambridge University Press

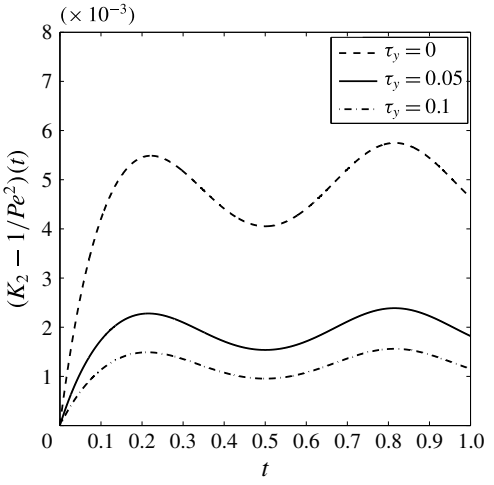


FIGURE 27. Variation of dispersion coefficient $(K_2 - 1/Pe^2)(t)$ with t for different values of τ_y when $\beta = 1$, $\alpha = 0.1$, $e = 0.1$ and $Sc = 1000$.

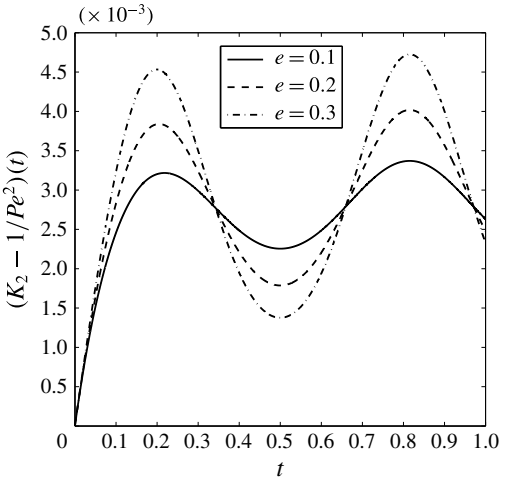


FIGURE 28. Variation of dispersion coefficient $(K_2 - 1/Pe^2)(t)$ with t for different values of e when $\tau_y = 0.02$, $\beta = 1$, $\alpha = 0.1$ and $Sc = 1000$.

figures 27–30. Comparison of the two calculations for the dispersion coefficient against the Womersley frequency parameter α between Sebastian & Nagarani (2015) and the present work revealed the following discrepancies.

It is seen from the figure (*a*) of Sebastian & Nagarani (2015) that K_2 becomes negative at large time $t = 1$ for $\tau_y = 0.1$, but the present investigation shows that dispersion coefficient is non-negative for those chosen values of the parameters (see figure 27). Similarly, as β increases in its range, K_2 is shown to decrease and become negative (see figure (*c*) of Sebastian & Nagarani (2015)). But it is noticed from the present investigation that as β increases, K_2 decreases but does not become negative for $\beta = 1$ at large time $t = 1$ and this decrement of K_2 is small for small values of β as shown in figure 29. The reason for decrement of dispersion coefficient has

https://doi.org/10.1017/jfm.2016.155 Published online by Cambridge University Press

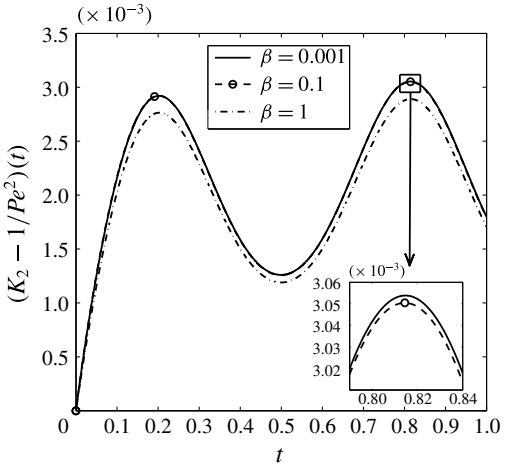


FIGURE 29. Variation of dispersion coefficient $(K_2 - 1/Pe^2)(t)$ with t for different values of β when $\tau_y = 0.05$, $\alpha = 0.1$, $e = 0.2$ and $Sc = 1000$.

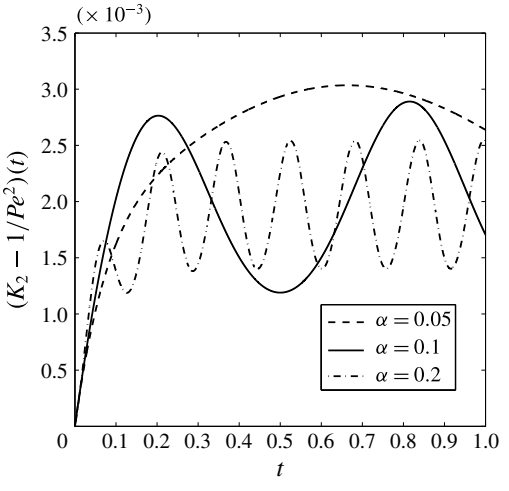


FIGURE 30. Variation of dispersion coefficient $(K_2 - 1/Pe^2)(t)$ with t for different values of α when $\tau_y = 0.05$, $\beta = 1$, $e = 0.2$ and $Sc = 1000$.

been discussed earlier in this study. Similar discrepancy is noticed for the dispersion coefficient K_2 when plotted against α, which are shown in figure (*d*) of Sebastian & Nagarani (2015) and figure 30 of the present investigation. The period of oscillation becomes shorter and K_2 reaches early a non-transient state as α increases. It is seen that for $\alpha = 0.2$, the amplitude of oscillations of K_2 becomes stable after four cycles of oscillation. But figure (*d*) of Sebastian & Nagarani (2015) indicated that K_2 decreases sharply at large time for $\alpha = 0.2$ and does not reach a stationary state at large time $(0.5 < t < 1)$. Figure 25 also shows that K_2 is positive for small value of α (say 0.1). This result is shown in three cycles of oscillation. As time increases, the amplitude of oscillations of K_2 increases and becomes stable at large time after first cycle of oscillation. All these above mentioned discrepancies are probably associated with the

https://doi.org/10.1017/jfm.2016.155 Published online by Cambridge University Press

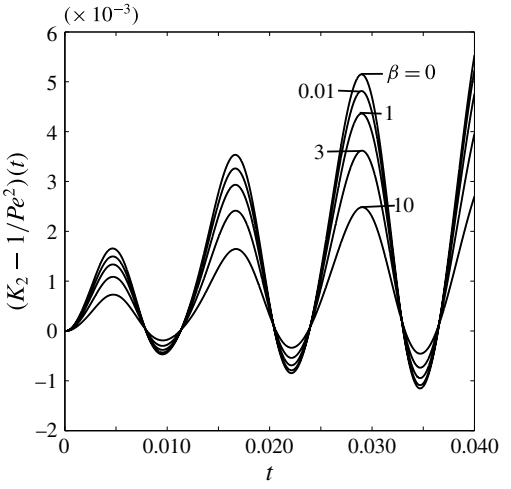


FIGURE 31. Variation of dispersion coefficient $(K_2 - 1/Pe^2)(t)$ for different values of β with small time t when $\tau_y = 0$, $e = 1.5$, $\alpha = 0.5$ and $Sc = 1000$.

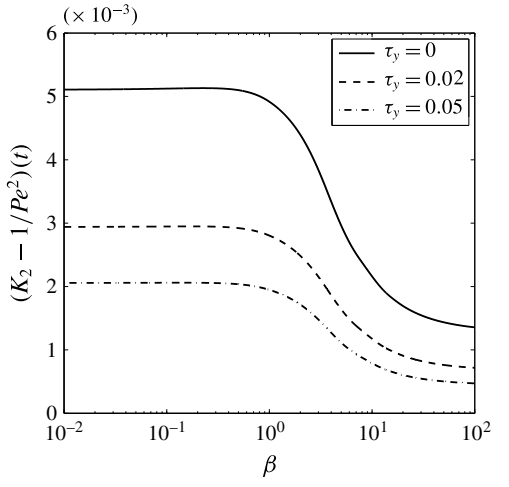


FIGURE 32. Variation of dispersion coefficient $(K_2 - 1/Pe^2)(t)$ for different values of τ_y with wall absorption parameter β at large time $t = 1$ when $e = 0$.

numerical treatment made in Sebastian & Nagarani (2015). Also, by considering $\tau_y = 0$ (Newtonian fluid case), the variation of K_2 with small time t for different values of β and $e = 1.5$ has been shown in figure 31. These results coincide exactly with those presented in figure 10 of Mazumder & Das (1992) for all values of β. To make this comparison, we set α as $\omega R^2/(\mu/\rho)$ instead of α^2 which is used throughout this investigation. This comparison also shows that the present results are consistent for small and large times.

Yet other comparison of the present results is made with Sankarasubramanian & Gill (1973) (see figure 4) and Nagarani *et al.* (2004) (see figure 4*a*), which are in the best agreement, for the variation of axial dispersion coefficient K_2 with β for different values of τ_y when $e = 0$ and time t is very large and is shown in figure 32. As β

https://doi.org/10.1017/jfm.2016.155 Published online by Cambridge University Press

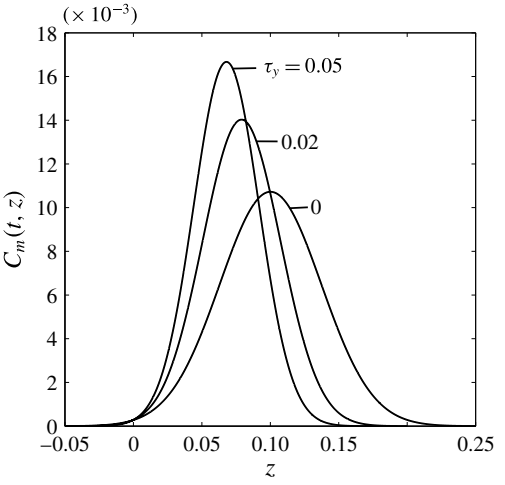


FIGURE 33. Variation of axial mean concentration $C_m(t, z)$ with axial distances z for different values of τ_y when $\beta = 0.01$, $t = 0.2$, $\alpha = 0.5$, $e = 0.5$ and $Sc = 1000$.

increases, K_2 decreases and it also decreases as τ_y increases. The physical reason for this behaviour is discussed already earlier in this paper. This comparison also reveals that the present results are reliable.

4.4. *Mean concentration* $C_m(t, z)$

The axial distribution of mean concentration C_m depends on the time t, yield stress τ_y, absorption parameter β, amplitude of the fluctuating pressure component e and frequency parameter α. In this study, the effects of t, τ_y, β, e and α on the axial distribution of mean concentration have been analysed. The equation (3.7) involving exchange coefficient K_0, convection coefficient K_1 and dispersion coefficient K_2 is solved to obtain the mean concentration C_m. From (3.47) and (3.48*a–c*), C_m is obtained and it directly depends on K_0, K_1 and K_2.

The distribution profiles of mean concentration C_m along the axial distance z with different τ_y have been shown in figure 33. The increase in the non-Newtonian nature of the fluid is seen to have increasing value of the mean concentration. It is seen that as τ_y increases, the peak of mean concentration increases. Due to increase in yield stress of the fluid, flow velocity decreases and hence decreases the solute dispersion. Therefore, the mean concentration of solute increases in the axial direction. Figure 34 shows the distribution of mean concentration along the axial distance z at different times t. It is noticed that as t increases, the peak of mean concentration decreases. Due to the presence of the boundary absorption at the tube wall, the solute in the system is continuously depleted and more amount of solute from the system is absorbed with the increasing of time t. So, the solute concentration decreases as time increases. At small time after the injection of solute in the system, solute dispersion is controlled by convection and the molecular diffusion is not quite effective. Hence, the distribution profile of mean concentration at small time ($t = 0.1$) is more peaky. As the time increases, the dispersion becomes diffusion controlled at large time ($t = 0.3$) and the concentration profile becomes more blunt and dispersed. From figure 35, it is noticed that as β increases, the peak of mean concentration decreases along the axial distance z. Due to increase in β, more amount of solute is supplied to conduct the

https://doi.org/10.1017/jfm.2016.155 Published online by Cambridge University Press

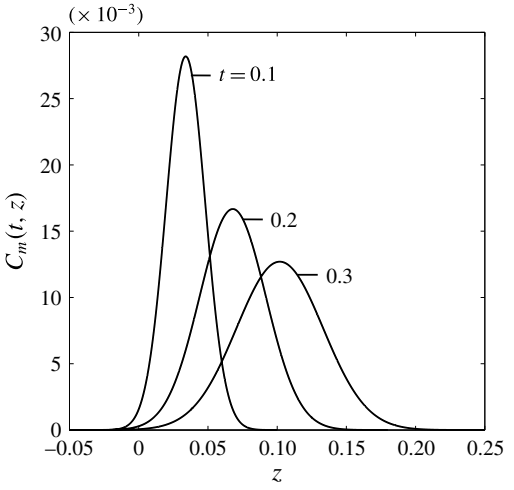


FIGURE 34. Variation of axial mean concentration $C_m(t, z)$ with axial distances z for different values of time t when $\tau_y = 0.05$, $\beta = 0.01$, $\alpha = 0.5$, $e = 0.5$ and $Sc = 1000$.

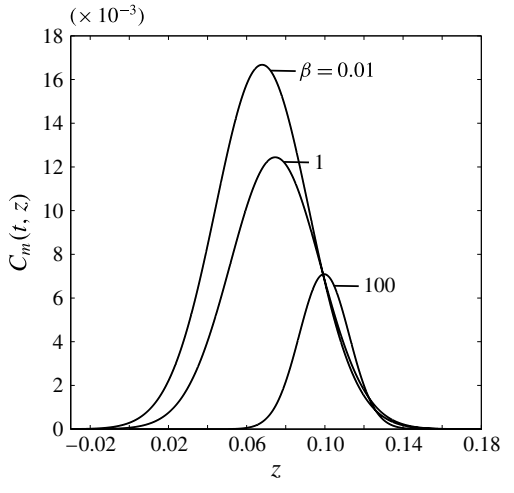


FIGURE 35. Variation of axial mean concentration $C_m(t, z)$ with axial distances z for different values of β when $t = 0.2$, $\alpha = 0.5$, $\tau_y = 0.05$, $e = 0.5$ and $Sc = 1000$.

boundary absorption or reaction at the tube wall and it reduces the concentration in the tube. From figure 36, it is observed that the peak of C_m decreases as e increases. As e increases, both the flow velocity and the dispersion coefficient increases. Hence it decreases the solute concentration. But the decrement of C_m is very small and it can be neglected. Figure 37 shows the axial distribution of mean concentration along the axial distance z with different values of α. It is seen that the peak of C_m increases with α but this increment is also very very small and it can be neglected.

When $e = 0$ and t is very large, the distribution profiles of mean concentration C_m at $z = 0.5$ with t for various values of β and τ_y are presented in figure 38. It is observed that as β increases, the peak of C_m decreases as also seen in Nagarani *et al.* (2004). The mean concentration C_m decreases with the time due to constant depletion

https://doi.org/10.1017/jfm.2016.155 Published online by Cambridge University Press

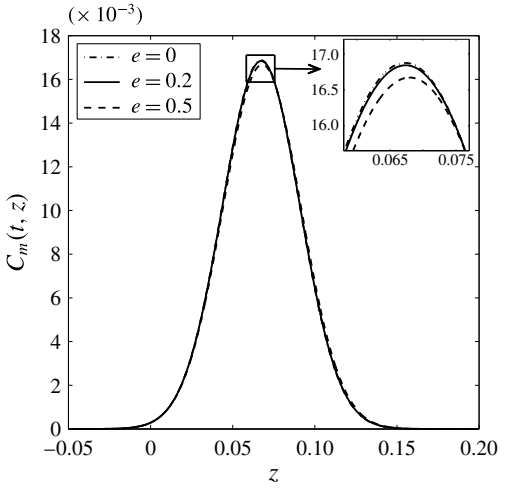


FIGURE 36. Variation of axial mean concentration $C_m(t, z)$ with axial distances z for different values of e when $t = 0.2$, $\beta = 0.01$, $\alpha = 0.5$, $\tau_y = 0.05$ and $Sc = 1000$.

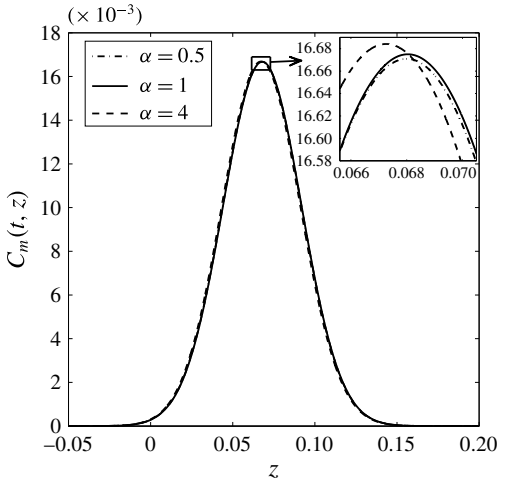


FIGURE 37. Variation of axial mean concentration $C_m(t, z)$ with axial distances z for different values of α when $t = 0.2$, $\beta = 0.01$, $e = 0.5$, $\tau_y = 0.05$ and $Sc = 1000$.

of solute occurring at the tube wall. These results are found to be in agreement with Sankarasubramanian & Gill (1973) for $\tau_y = 0$ and Nagarani *et al.* (2004).

5. Conclusions

In this analysis, the effect of catalytic reaction at the tube wall on axial dispersion of solute in a periodic flow of Casson fluid is discussed with the pulsatile pressure gradient by applying the generalized dispersion model. The three effective transport coefficients i.e. exchange, convective and dispersion coefficients are determined to analyse the axial dispersion and axial mean concentration of solute in the presence of the boundary absorption at the tube wall. It is observed that exchange coefficient

https://doi.org/10.1017/jfm.2016.155 Published online by Cambridge University Press

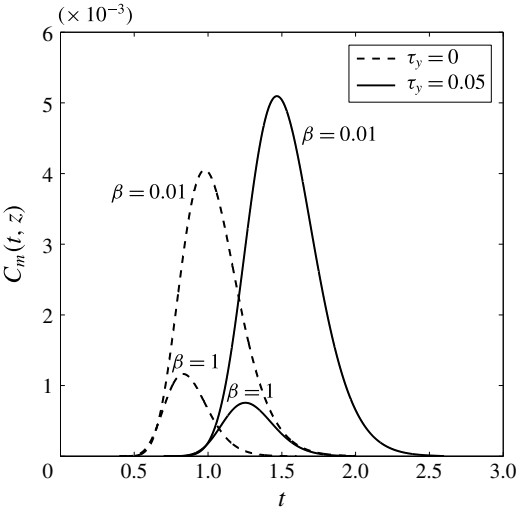


FIGURE 38. Variation of axial mean concentration $C_m(t, z)$ with time t for different values of τ_y and β at large time $t = 1$ when $e = 0$ and $z = 0.5$.

K_0 depends on time t and wall absorption parameter β but the convective coefficient K_1 and dispersion coefficient K_2 depend on time t, wall absorption parameter β, yield stress of the fluid τ_y, the fluctuating pressure component e and Womersley frequency parameter α. The results of K_0, K_1, K_2 and C_m for a Newtonian fluid at large time are found to be in best agreement with Sankarasubramanian & Gill (1973) and Nagarani *et al.* (2004). As τ_y increases, the amplitude of fluctuations and the magnitude of both negative convective coefficient $-K_1$ and dispersion coefficient K_2 decreases. In this study, it is seen that the amplitude of fluctuations of both $-K_1$ and K_2 increases with e. As β increases, K_1 and K_2 increases and decreases, respectively. As α increases, the amplitude of oscillations of K_2 decreases. At small time, K_2 increases cyclically with the period of oscillation and becomes stable at large time. It is observed that the critical time for which K_2 reaches a non-transient state is independent of τ_y and e of the fluid but dependent of α. For small α, K_2 oscillates with single frequency period at small time but for large α, it begins to oscillate at small time with double frequency period. As α increases, K_2 fluctuates in shorter period of oscillation. For large values of α, K_2 becomes positive and negative during the cycle of oscillation and this phenomena also depends on τ_y, e and β. The peak of axial mean concentration C_m increases with τ_y. As the time t increases after the injection of solute, the peak of C_m decreases and becomes flat. It is also seen that the peak of C_m decreases with increment of β. For the variation of e and α, there is not significant change in axial distribution of mean concentration C_m and it can be neglected.

Acknowledgements

The authors are thankful to all the reviewers for their valuable comments and constructive criticism for the improvement of the technical content of the manuscript.

https://doi.org/10.1017/jfm.2016.155 Published online by Cambridge University Press

REFERENCES

AGRAWAL, S. & JAYARAMAN, G. 1994 Numerical simulation of dispersion in the flow of power law fluids in curved tubes. *Appl. Math. Model.* **18** (9), 504–512.

ARIS, R. 1956 On the dispersion of a solute in a fluid flowing through a tube. *Proc. R. Soc. Lond.* A **235** (1200), 67–77.

ARIS, R. 1960 On the dispersion of a solute in pulsating flow through a tube. *Proc. R. Soc. Lond.* A **259** (1298), 370–376.

AROESTY, J. & GROSS, J. F. 1972 The mathematics of pulsatile flow in small vessels: I. Casson theory. *Microvasc. Res.* **4** (1), 1–12.

BANDYOPADHYAY, S. & MAZUMDER, B. S. 1999 Unsteady convective diffusion in a pulsatile flow through a channel. *Acta Mechanica* **134** (1–2), 1–16.

BOYCE, W. E, DIPRIMA, R. C. & HAINES, C. W. 1992 *Elementary Differential Equations and Boundary Value Problems*. Wiley.

BRONZINO, J. D. 1999 *Biomedical Engineering Handbook*. CRC Press.

CARO, C. G., PEDLEY, T. J., SCHROTER, R. C. & SEED, W. A. 1978 *The Mechanics of the Circulation*. Oxford University Press.

CHANDRAN, K. B., RITTGERS, S. E. & YOGANATHAN, A. P. 2012 *Biofluid Mechanics: The Human Circulation*. CRC Press.

CHATWIN, P. C. 1975 On the longitudinal dispersion of passive contaminant in oscillatory flows in tubes. *J. Fluid Mech.* **71** (03), 513–527.

CRACIUNESCU, O. I. & CLEGG, S. T. 2001 Pulsatile blood flow effects on temperature distribution and heat transfer in rigid vessels. *J. Biomech. Engng* **123** (5), 500–505.

DASH, R. K., JAYARAMAN, G. & MEHTA, K. N. 1996 Estimation of increased flow resistance in a narrow catheterized artery – a theoretical model. *J. Biomech.* **29** (7), 917–930.

DASH, R. K., JAYARAMAN, G. & MEHTA, K. N. 2000 Shear augmented dispersion of a solute in a Casson fluid flowing in a conduit. *Ann. Biomed. Engng* **28** (4), 373–385.

GILL, W. N. & SANKARASUBRAMANIAN, R. 1970 Exact analysis of unsteady convective diffusion. *Proc. R. Soc. Lond.* A **316** (1526), 341–350.

HAZRA, S. B., GUPTA, A. S. & NIYOGI, P. 1997 On the dispersion of a solute in oscillating flow of a non-newtonian fluid in a channel. *Heat Mass Transfer* **32** (6), 481–488.

JOSHI, C. H., KAMM, R. D., DRAZEN, J. M. & SLUTSKY, A. S. 1983 An experimental study of gas exchange in laminar oscillatory flow. *J. Fluid Mech.* **133**, 245–254.

KAYE, S. R., KAVAFYAN, P. & SCHROTER, R. C. 1993 Dispersion and uptake in a coiled tube. *J. Biomech. Engng* **115** (1), 125–126.

KU, D. N. 1997 Blood flow in arteries. *Annu. Rev. Fluid Mech.* **29** (1), 399–434.

KUMAR, S. & JAYARAMAN, G. 2008 Method of moments for laminar dispersion in an oscillatory flow through curved channels with absorbing walls. *Heat Mass Transfer* **44** (11), 1323–1336.

MAZUMDER, B. S. & DAS, S. K. 1992 Effect of boundary reaction on solute dispersion in pulsatile flow through a tube. *J. Fluid Mech.* **239**, 523–549.

MAZUMDER, B. S. & MONDAL, K. K. 2005 On solute transport in oscillatory flow through an annular pipe with a reactive wall and its application to a catheterized artery. *Q. J. Mech. Appl. Maths* **58** (3), 349–365.

MERRILL, E. W. 1969 Rheology of blood. *Phys. Rev.* **49** (4), 863–888.

NAGARANI, P., SAROJAMMA, G. & JAYARAMAN, G. 2004 Effect of boundary absorption in dispersion in Casson fluid flow in a tube. *Ann. Biomed. Engng* **32** (5), 706–719.

NAGARANI, P., SAROJAMMA, G. & JAYARAMAN, G. 2006 Exact analysis of unsteady convective diffusion in Casson fluid flow in an annulus–application to catheterized artery. *Acta Mechanica* **187** (1–4), 189–202.

NAGARANI, P., SAROJAMMA, G. & JAYARAMAN, G. 2009 Effect of boundary absorption on dispersion in Casson fluid flow in an annulus: application to catheterized artery. *Acta Mechanica* **202** (1–4), 47–63.

NAGARANI, P. & SEBASTIAN, B. T. 2013 Dispersion of a solute in pulsatile non-newtonian fluid flow through a tube. *Acta Mechanica* **224** (3), 571–585.

https://doi.org/10.1017/jfm.2016.155 Published online by Cambridge University Press

NG, C. O. 2006 Dispersion in steady and oscillatory flows through a tube with reversible and irreversible wall reactions. *Proc. R. Soc. Lond.* A **462** (2066), 481–515.

PAUL, S. 2011 Effect of wall oscillation on dispersion in axi-symmetric flows between two coaxial cylinders. *Z. Angew. Math. Mech.* **91** (1), 23–37.

RAO, A. R. & DESHIKACHAR, K. S. 1987 An exact analysis of unsteady convective diffusion in an annular pipe. *Z. Angew. Math. Mech.* **67** (3), 189–195.

SANKARASUBRAMANIAN, R. & GILL, W. N. 1973 Unsteady convective diffusion with interphase mass transfer. *Proc. R. Soc. Lond.* A **333** (1592), 115–132.

SARKAR, A. & JAYARAMAN, G. 2004 The effect of wall absorption on dispersion in oscillatory flow in an annulus: application to a catheterized artery. *Acta Mechanica* **172** (3–4), 151–167.

SEBASTIAN, B. T. & NAGARANI, P. 2015 Effect of boundary absorption on dispersion of a solute in pulsatile Casson fluid flow. *Interdiscip. Top. Appl. Math. Model. Comput. Sci.* 389–395.

SHARP, M. K. 1993 Shear-augmented dispersion in non-newtonian fluids. *Ann. Biomed. Engng* **21** (4), 407–415.

SMITH, R. 1982 Contaminant dispersion in oscillatory flows. *J. Fluid Mech.* **114**, 379–398.

TAYLOR, G. 1953 Dispersion of soluble matter in solvent flowing slowly through a tube. *Proc. R. Soc. Lond.* A **219** (1137), 186–203.

TRUSKEY, G. A., YUAN, F. & KATZ, D. F. 2004 *Transport Phenomena in Biological Systems*. Pearson Prentice Hall.

https://doi.org/10.1017/jfm.2016.155 Published online by Cambridge University Press